Models of lithosphere and asthenosphere anisotropic structure of the Yellowstone hot spot from shear wave splitting

Gregory P. Waite[1]
Department of Geology and Geophysics, University of Utah, Salt Lake City, Utah, USA

Derek L. Schutt
Department of Geology and Geophysics, University of Wyoming, Laramie, Wyoming, USA

Robert B. Smith
Department of Geology and Geophysics, University of Utah, Salt Lake City, Utah, USA

Received 27 October 2004; revised 15 April 2005; accepted 8 August 2005; published 8 November 2005.

[1] Teleseismic shear wave splitting measured at 56 continuous and temporary seismographs deployed in a 500 km by 600 km area around the Yellowstone hot spot indicates that fast anisotropy in the mantle is parallel to the direction of plate motion under most of the array. The average split time from all stations of 0.9 s is typical of continental stations. There is little evidence for plume-induced radial strain, suggesting that any contribution of gravitationally spreading plume material is undetectably small with respect to the plate motion velocity. Two stations within Yellowstone have splitting measurements indicating the apparent fast anisotropy direction (ϕ) is nearly perpendicular to plate motion. These stations are ~30 km from stations with ϕ parallel to plate motion. The 70° rotation over 30 km suggests a shallow source of anisotropy; however, split times for these stations are more than 2 s. We suggest melt-filled, stress-oriented cracks in the lithosphere are responsible for the anomalous ϕ orientations within Yellowstone. Stations southeast of Yellowstone have measurements of ϕ oriented NNW to WNW at high angles to the plate motion direction. The Archean lithosphere beneath these stations may have significant anisotropy capable of producing the observed splitting.

Citation: Waite, G. P., D. L. Schutt, and R. B. Smith (2005), Models of lithosphere and asthenosphere anisotropic structure of the Yellowstone hot spot from shear wave splitting, *J. Geophys. Res.*, *110*, B11304, doi:10.1029/2004JB003501.

1. Introduction

[2] The Yellowstone Plateau volcanic field in northwestern Wyoming is the youngest manifestation of the Yellowstone hot spot. Three large, caldera-forming explosions at Yellowstone in the past 2 Myr, as well as numerous flows between each of the caldera-forming events, have erupted as much as 6500 km^3 of rhyolite and basalt [*Christiansen*, 2001]. Beginning at the youngest, 0.64 Ma caldera at the Yellowstone volcanic field, an 800 km line of progressively older eruptive centers extends SW along the eastern Snake River Plain (ESRP) to the 16 Ma McDermitt volcanic field on the Oregon-Nevada border [*Christiansen and Yeats*, 1992]. *Perkins and Nash* [2002] identified 142 ash fall eruptions from Yellowstone, each of which may represent an explosive caldera-forming eruption along the hot spot track.

[3] The rate and direction of the progression of the hot spot across the southwesterly moving North America plate are consistent with a persistent, stationary, sublithospheric source. Yellowstone has been viewed as the archetypical continental hot spot primarily because of four characteristics that suggest a mantle source: (1) the well-defined track of progressively older silicic volcanism in the direction of plate motion; (2) a parabolic pattern of high topography (>1000 m) and seismicity around the aseismic and topographically low ESRP with its apex at the Yellowstone plateau [*Smith and Sbar*, 1974; *Anders et al.*, 1989; *Pierce and Morgan*, 1992; *Smith and Braile*, 1994]; (3) high ^{3}He/^{4}He ratios suggestive of a primordial mantle source [*Craig et al.*, 1978]; and (4) a 10 to 12 m positive geoid anomaly with a ~500 km radius, comparable to that of Hawaii, centered at Yellowstone [*Smith and Braile*, 1994; *Smith and Milbert*, 1999].

[4] Local features of the Yellowstone Plateau demonstrate the dynamic nature of the hot spot at its present location. Regional heat flow at Yellowstone, estimated at more than 1700 mW/m^2 [*Blackwell*, 1969], is the highest in North America [see, e.g., *Goes and van der Lee*, 2002]. High heat flow has been attributed to crystallization and cooling of rhyolitic magma [*Fournier and Pitt*, 1985] or basaltic magma intruded from the upper mantle [e.g., *Christiansen*, 2001]. A ~60 mGal gravity anomaly that is roughly within the youngest 0.64 Ma caldera is interpreted as a hot, shallow

[1]Now at U.S. Geological Survey, Menlo Park, California, USA.

0148-0227/05/2004JB003501$09.00

granitic batholith [*Lehman et al.*, 1982]. *Evoy* [1978] inverted teleseismic *P* wave delays and gravity jointly to reveal a low V_P, low-density body extending to at least 100 km depth. Some degree of melt beneath the Yellowstone caldera is required to explain the gravity and *P* wave delays [*Evoy*, 1978]. Likewise, a small percentage of partial melt has been interpreted to exist in the upper mantle beneath the ESRP ~200 km SW of Yellowstone [*Schutt and Humphreys*, 2004].

[5] A low (−8%) V_P body in the upper crust beneath the caldera has been imaged by local earthquake tomography [*Benz and Smith*, 1984; *Miller and Smith*, 1999; *Husen et al.*, 2004]. This seismic anomaly has been interpreted as a hot body with up to a few percent partial melt [*Miller and Smith*, 1999; *Husen et al.*, 2004]. Intense swarms and the largest historic earthquake in the Cordillera, the M_S7.5 1959 Hebgen Lake earthquake, characterize local seismicity. Crustal deformation measurements have documented periods of uplift and subsidence within and adjacent to the caldera [e.g., *Pelton and Smith*, 1982; *Wicks et al.*, 1998; *Puskas et al.*, 2002]. These local features are ultimately due to an influx of heat from the mantle [e.g., *Smith and Braile*, 1994; *Christiansen*, 2001].

[6] Traditionally, the evidence has pointed to a mantle plume source for the Yellowstone hot spot [e.g., *Morgan*, 1971; *Smith and Sbar*, 1974; *Duncan and Richards*, 1991; *Anders and Sleep*, 1992; *Pierce and Morgan*, 1992; *Bijwaard et al.*, 1998; *Steinberger*, 2000]. In this paper, a plume is defined generally as a near-vertical, approximately axisymmetric, buoyant upwelling arising from an unspecified depth in the mantle. Some researchers have suggested there is not definitive evidence for or against a mantle plume [e.g., *Smith and Braile*, 1994; *Humphreys et al.*, 2000], while others have argued against a plume source [e.g., *Favela and Anderson*, 2000; *Christiansen et al.*, 2002].

[7] Perhaps the most compelling evidence against a plume source for Yellowstone has been the lack of a clear seismic image of the plume in regional *P* wave tomography studies [*Evans and Iyer*, 1979; *Iyer et al.*, 1981; *Dueker and Humphreys*, 1990; *Humphreys and Dueker*, 1994a, 1994b; *Christiansen et al.*, 2002]. While these studies show a low-velocity anomaly to at least 200 km depth, the limitations in the data may preclude resolution of deeper anomalies.

[8] Global *P* wave tomography models by *Bijwaard et al.* [1998] and *Montelli et al.* [2004] reveal a low-velocity anomaly to at least 650 km beneath Yellowstone. *Bijwaard et al.* [1998] interpret the anomaly as a plume. However, *Montelli et al.* [2004], seeing no evidence for continuation of the anomaly through the lower mantle to the core-mantle boundary, do not interpret the Yellowstone anomaly as a plume. Uncorrelated 410 and 660 km discontinuity topography beneath Yellowstone argues against a vertically coherent thermal plume through the mantle transition zone [*Fee and Dueker*, 2004].

[9] New tomography studies employing an expansive data set of teleseismic *P* and *S* wave records from seismographs deployed for the same project that provided the data for this paper indicate strong low *P* and *S* wave velocity anomalies are present to ~250 km directly beneath Yellowstone. A weaker anomaly continues down to at least the 410 km discontinuity at a point 100 km NW of Yellowstone [*Waite et al.*, 2003; *Jordan et al.*, 2004]. These data resolve a plume through the upper mantle that may be entrained in local or regional mantle flow.

[10] Studies of shear wave anisotropy have been used to test models of the upper mantle strain field predicted to result from buoyant plumes [e.g., *Rümpker and Silver*, 2000; *Walker et al.*, 2001; *Kaminski and Ribe*, 2002]. The combination of radial flow of plume material at the base of the plate with shear by the moving plate over the relatively stationary mantle is expected to produce a parabolic pattern of asthenosphere flow [e.g., *Sleep*, 1990]. This mantle flow pattern should be reflected in the anisotropic fabric around the hot spot. Parabolic patterns of shear wave anisotropy measured by shear wave splitting have been attributed to plume-plate interaction at the Hawaii and Eifel hot spots [*Walker et al.*, 2001, 2003; *Bokelmann et al.*, 2003].

[11] A significant mantle plume should produce a similar parabolic flow pattern at Yellowstone. For example, the parabolic pattern of high topography and seismicity that surrounds the Snake River Plain has been attributed to plume-lithosphere interaction [e.g., *Anders et al.*, 1989; *Smith and Braile*, 1994; *Lowry et al.*, 2000]. Shear wave splitting measurements can be used to resolve the anisotropic fabric expected to be produced by mantle flow. For this purpose, we measure splitting of core-refracted mantle phases *SKS*, *SKKS*, and *PKS* from earthquakes recorded on arrays of permanent and temporary broadband stations around Yellowstone.

2. Methods for Measuring Shear Wave Splitting

[12] Seismic anisotropy was estimated from birefringence of teleseismic shear waves recorded at distances of 60° to 180°. We used the methodology of *Silver and Chan* [1991] to estimate the azimuth of the shear wave polarization with the maximum velocity, ϕ, and the accumulated arrival time difference between the fast and slow polarized waves, δt. The splitting parameters (ϕ and δt) that minimize energy on the tangential component (E_t) are the best fitting parameters. We also employed the method of *Levin et al.* [1999], which uses cross correlation between the radial and tangential traces to estimate the splitting parameters. These methods assume that a single layer of transversely anisotropic material with hexagonal symmetry produces the splitting. Because of this assumption, the modeled splitting parameters are referred to as ''apparent'' splitting parameters.

[13] *Silver and Chan* [1991] show that $E_t(\phi, \delta t)$ can be regarded as a χ^2 variable, so estimates of the uncertainties can be made with *F* test statistics. The method of *Silver and Chan* [1991] has been shown to underestimate errors for noisy data [*Sandvol and Hearn*, 1994] because it allows E_t to be reduced below the noise level. To prevent this problem, we used a modified version of *Silver and Chan* [1991] that prevents minimization of E_t below the noise level.

[14] The method of *Levin et al.* [1999] uses cross correlation of the radial and tangential traces to find the best estimates of the splitting parameters over the same grids of possible values. It assumes the split *S* wave is composed of two pulses with the similar shapes that are shifted in time by $\pm 1/2\ \delta t$ and have orthogonal polarization.

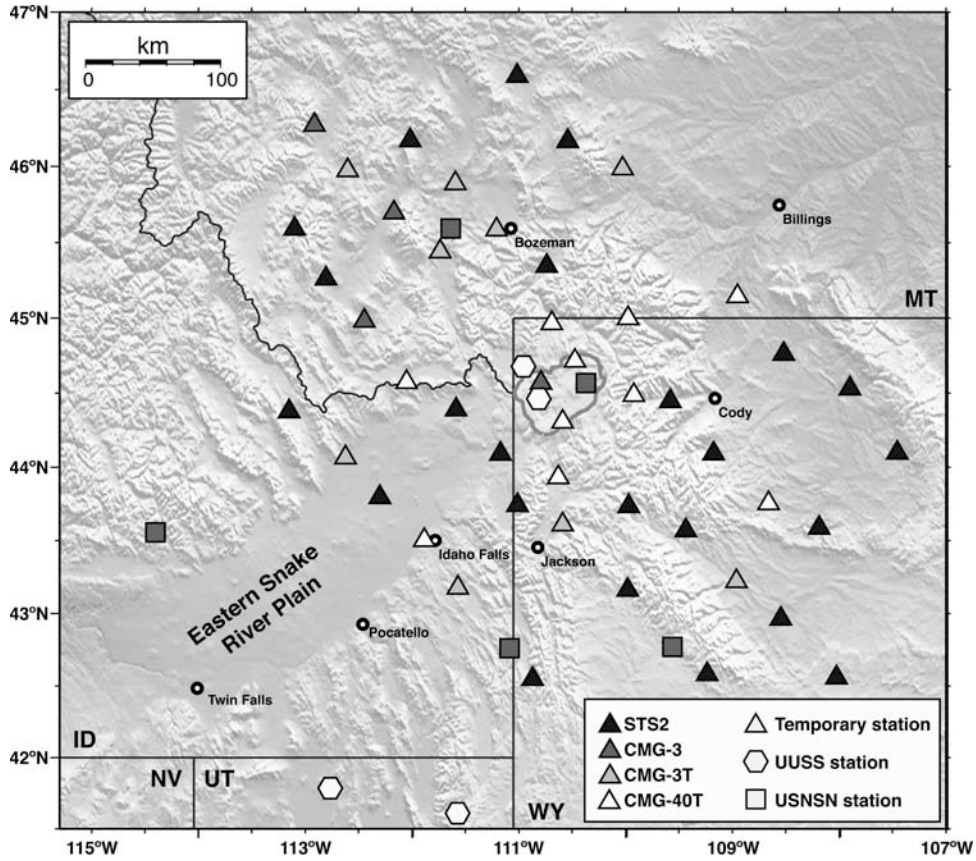

Figure 1. Seismographs used in the study. The temporary array is made up of five lines oriented NW-SE. Additional stations are part of USNSN and UUSS permanent networks. Symbols indicate station owner and are shaded by sensor type. State boundaries, selected cities, and the 0.6 Ma caldera are shown for reference.

The apparent splitting parameters that produce the highest cross-correlation coefficient are best. Error estimates are made using the curvature of the cross-correlation function at the maximum following *Menke* [1989].

[15] Some waveforms have little to no energy on the tangential component indicating no splitting of radial energy. This can occur if there is no anisotropy along the ray path or if either the fast or slow axis of anisotropy is aligned with the plane containing the ray. These so-called "null" splits can be useful in constraining the direction of fast anisotropy if they are combined with observations of split *S* waves from other azimuths. We extended the *Silver and Chan* [1991] method to "station average" split parameters following *Schutt et al.* [1998]. Station averages are formed from the sum of the corrected energy for all ϕ and δt, for all events at a given station. The ϕ and δt that give the minimum from that sum are the best fit parameters. Since the sum of χ^2 variables is itself χ^2 distributed, error estimates for station averages can be made using essentially the same *F* test statistics.

[16] Station averages are particularly useful when working with temporary arrays. A station operating for less than a year may only record a small number of useful *SKS* phases and many records may have a low signal-to-noise ratio. By summing the E_t for all events at a station, the signal-to-noise ratio is effectively improved. However, this method is only valid for near-vertical rays transmitted through an anisotropic layer where the fast polarization direction is horizontal. This may not be the case for all stations in this array. For example, if the fast axis of anisotropy is subhorizontal, the apparent splitting parameters will vary with earthquake back azimuth [e.g., *Crampin and Booth*, 1985]. Similarly, the apparent splitting parameters will vary with back azimuth if there are multiple layers of anisotropy [e.g., *Silver and Savage*, 1994].

3. Shear Wave Splitting at the Yellowstone Hot Spot

3.1. Data Analysis

[17] Seismic data used in this research came from three sources: a temporary deployment of 47 broadband seismographs deployed specifically for this study, four broadband stations in the University of Utah Seismograph Stations (UUSS) permanent network in Yellowstone and Utah, and five broadband stations in the U.S. National Seismograph Network (USNSN) (Figure 1). Up to 5 years of recordings, 1999 through 2003, from the permanent network stations were included. The temporary network was deployed in June 2000 and removed in May and June 2001. The Incorporated Research Institutions for Seismology (IRIS) Program for the Array Seismic Studies of the Continental

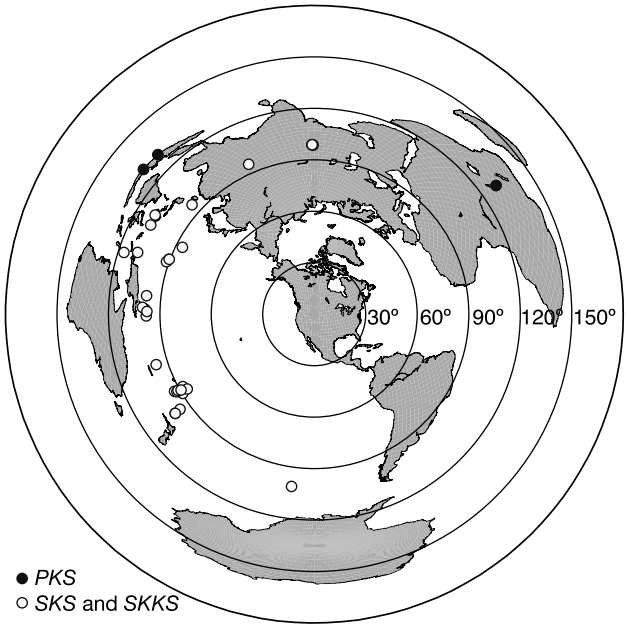

Figure 2. Locations of earthquake epicenters used in the splitting analysis. The map is centered on Yellowstone. *SKS*, *SKKS*, and *PKS* phases were used.

Lithosphere (PASSCAL) provided the instruments. Data were recorded using four different types of three-component, broadband seismometers: Güralp CMG-40T, CMG-3ESP, CMG-3T, and Streckeisen STS-2. The temporary arrays used RefTek 72 series digitizer recorders.

[18] Each *SKS* record from earthquakes of magnitude 5.6 or larger was examined for clear *SKS* arrivals. *SKS* is present at distances from 61°, for deep focus earthquakes, to 144°, for surface focus events. In practice, the proximate arrival of direct *S* and *ScS* at distances up to about 85° contaminate the *SKS* and make them unusable for splitting analysis. A time window of 20 to 35 s was selected around each phase, depending on the presence of other phases, and the data were band pass filtered between 1 s and 30 s. Each phase was analyzed with both the *Silver and Chan* [1991] and *Levin et al.* [1999] methods described above.

[19] For well-resolved phases, the two methods produce results that are insignificantly different at the 95% confidence interval. The agreement of two independent techniques provides confidence in the results. However, the *Levin et al.* [1999] method does not resolve splitting well when there is little energy on the tangential component. Data were sorted to remove events with 2σ errors in $\delta t > 1.05$ s and 2σ errors in $\phi > 35°$. Where the splitting parameters produced by the two different methods agree, they are judged high quality (A). In cases where results of the different methods do not agree, the results are carefully reviewed. They are included in the data set as good quality (B) if they show initial elliptical particle motion and the *Levin et al.* [1999] method results are within the 99% confidence bounds computed with the *Silver and Chan* [1991] method.

[20] The majority of events with good *SKS* phases originated in circum-Pacific subduction zones with back azimuths from SW through NW (Figure 2). In order to improve the azimuthal distribution of the data set, we searched for additional *PKS* and *SKKS* phases from events at different back azimuths. The *SKKS* phase is found at distances out to 180° providing a greater set of possible events to use. The *PKS* phase is found at distances that overlap with the *SKS*, but can be useful where the geometry of the main fault planes in a particular seismogenic zone results in little *S* energy radiating toward our study area. All but one of the *SKKS* phases examined had low signal-to-noise ratios (<2) or the splitting parameters had large errors so they were not useful for examining individual splits. Four earthquakes with *PKS* phases from distances of 130° to 133° were found to be useful including one event with a NE back azimuth. The locations of all 91 earthquakes used in the splitting analysis are shown in Figure 2, and they are listed in Table 1.

[21] Station average splitting parameters were computed from the individual event results by summing the corrected energy for all events at a given station, and finding the minimum from that sum as described above. The signal-to-noise ratio of each waveform used in the station averaging was required to be greater than 2. Station averaging permits the use of data that have poorly resolved splitting parameters, but obvious split shear waves. They are particularly useful for noisy or temporary stations that have no well-resolved single-event split parameters. However, stations with several pairs of split parameters that have strong back-azimuthal dependence are not good candidates for station averaging. Individual event splitting parameters were examined first and candidates for station average analysis were identified.

3.2. Individual Shear Wave Splitting Results

[22] A previous study of shear wave splitting across the ESRP (the track of the Yellowstone hot spot) 200 km SW of Yellowstone showed remarkable consistency in fast polarization direction over several hundred kilometers (Figure 3) [*Schutt et al.*, 1998; *Schutt and Humphreys*, 2001]. With the exception of a few stations on the ends of the array, fast directions are parallel to the direction of absolute plate motion (APM). Schutt and colleagues suggest that the North America plate in the wake of the Yellowstone hot spot was warmed as it passed over the hot spot allowing asthenosphere material to be easily reoriented by plate motion induced shear. Individual shear wave splitting results from the Yellowstone area are more varied. Table 2 lists the high-quality splitting results for each station. These results are plotted in Figure 3 along with the results from *Schutt et al.* [1998] for the ESRP.

[23] Our results from stations on or adjacent to the ESRP are generally consistent with the splits found by *Schutt et al.* [1998]. An example of diagnostic plots for a high-quality split for station Y03, on the ESRP, is shown in Figure 4. In the mountainous region north of Yellowstone and the ESRP, splits are not of high quality and several stations have only one or two well-constrained null splits. The null splits are consistent with a fast direction parallel to the APM direction ($249.5° \pm 10.7°$) [*Gripp and Gordon*, 2002]. However, station Y23 at the northwest end of the array has one split with $\phi = 10°$ and station Y38 has a split with $\phi = 90°$. While the uncertainty in the measurement at Y38 is large, the Y23 split is tightly constrained. The other two stations in this

Table 1. Events Used for Shear Wave Splitting Analysis

Year-Day	Latitude	Longitude	BAZ[a]	Phase	Number of Stations
1999-087	30.49°	79.29°	351°	*SKS*	5
1999-095	−5.31°	149.84°	271°	*SKS*	3
1999-103	−21.38°	−176.54°	238°	*SKS*	1
1999-110	−31.83°	−179.07°	232°	*SKS*	3
1999-126	29.50°	51.81°	16°	*SKS*	1
1999-137	−4.56°	152.96°	270°	*SKS*	3
1999-169	5.46°	126.66°	295°	*SKS*	1
1999-190	−6.54°	154.86°	267°	*SKS*	1
1999-199	−22.21°	179.26°	240°	*SKS*	1
1999-200	−28.58°	−177.61°	233°	*SKS*	3
1999-209	−30.24°	−177.98°	232°	*SKS*	2
1999-213	−30.44°	−177.84°	232°	*SKS*	3
1999-234	−16.10°	167.93°	251°	*SKS*	1
2000-005	−11.30°	165.37°	257°	*SKS*	2
2000-013	−17.50°	−178.91°	242°	*SKS*	1
2000-037	−5.86°	150.83°	271°	*SKS*	1
2000-056	−19.56°	173.78°	245°	*SKS*	1
2000-057	13.94°	144.65°	289°	*SKS*	4
2000-159	26.79°	97.29°	332°	*SKS*	2
2000-161	30.52°	137.76°	305°	*SKS*	2
2000-162	23.77°	121.12°	312°	*SKS*	2
2000-168	−33.89°	−70.00°	146°	*SKS*	1
2000-173	14.19°	144.79°	290°	*SKS*	4
2000-197	−7.03°	128.93°	287°	*SKS*	20
2000-198	−7.75°	150.92°	272°	*SKS*	2
2000-198	−4.19°	138.91°	281°	*SKS*	15
2000-199	36.21°	71.00°	304°	*SKS*	33
2000-199	36.28°	70.92°	307°	*SKS*	7
2000-204	−4.07°	102.37°	315°	*PKS*	1
2000-206	−5.56°	102.89°	313°	*PKS*	1
2000-216	−12.04°	166.45°	257°	*SKS*	8
2000-228	−31.51°	179.73°	234°	*SKS*	34
2000-228	−31.51°	179.73°	234°	*SKS*	15
2000-234	−53.08°	−46.32°	144°	*SKS*	6
2000-246	−17.92°	−178.32°	242°	*SKS*	6
2000-256	35.39°	99.34°	337°	*SKS*	7
2000-256	−5.43°	101.82°	315°	*PKS*	15
2000-261	−5.36°	146.76°	275°	*SKS*	18
2000-276	−7.98°	30.71°	54°	*PKS*	18
2000-278	−15.37°	166.91°	254°	*SKS*	39
2000-299	−6.55°	105.63°	309°	*PKS*	18
2000-299	−6.55°	105.63°	308°	*SKS*	10
2000-303	−4.77°	153.95°	270°	*SKS*	1
2000-328	−4.59°	153.06°	271°	*SKS*	11
2000-330	40.17°	49.95°	14°	*SKS*	4
2000-341	39.69°	54.86°	10°	*SKS*	2
2000-356	−5.71°	151.12°	272°	*SKS*	11
2000-356	−5.35°	154.13°	269°	*SKS*	1
2001-002	6.75°	126.81°	299°	*SKS*	5
2001-009	−14.93°	167.17°	255°	*SKS*	1
2001-026	23.40°	70.32°	239°	*SKS*	3
2001-044	−4.68°	102.56°	315°	*PKS*	14
2001-055	1.27°	126.25°	294°	*SKS*	2
2001-118	−18.06°	−176.94°	241°	*SKS*	18
2001-129	−10.32°	161.23°	261°	*SKS*	1
2001-139	−19.90°	−177.51°	242°	*SKS*	1
2001-143	−17.71°	−178.70°	242°	*SKS*	10
2001-154	−29.67°	−178.63°	234°	*SKS*	2
2001-184	21.61°	143.02°	296°	*SKS*	7
2001-185	−21.70°	−176.73°	238°	*SKS*	2
2001-189	−6.66°	152.01°	270°	*SKS*	1
2001-218	−55.59°	−123.16°	186°	*SKS*	2
2001-254	−0.56°	133.17°	287°	*SKS*	3
2001-255	−20.96°	−179.16°	239°	*SKS*	4
2001-285	12.59°	144.94°	288°	*SKS*	6
2001-294	−36.99°	179.02°	231°	*SKS*	1
2001-304	−5.88°	149.81°	273°	*SKS*	1
2001-309	−17.09°	−179.33°	243°	*SKS*	3
2001-346	−17.20°	167.70°	251°	*SKS*	2
2001-352	23.95°	122.88°	311°	*SKS*	5
2002-001	6.30°	125.65°	299°	*SKS*	1
2002-002	−17.78°	167.83°	251°	*SKS*	4
2002-022	35.73°	26.70°	33°	*SKS*	6
2002-062	36.44°	70.45°	358°	*SKS*	5
2002-085	23.54°	123.91°	311°	*SKS*	6
2002-116	13.09°	144.62°	289°	*SKS*	3
2002-128	−17.95°	−174.57°	239°	*SKS*	1
2002-173	35.63°	49.05°	14°	*SKS*	1
2002-181	−22.20°	179.25°	240°	*SKS*	6
2002-231	−21.70°	−179.51°	239°	*SKS*	6
2002-251	−3.30°	142.95°	278°	*SKS*	5
2003-124	−30.53°	−178.23°	233°	*SKS*	6
2003-133	−17.29°	167.74°	251°	*SKS*	5
2003−146	6.76°	123.71°	300°	*SKS*	7
2003-158	−5.09°	152.50°	270°	*SKS*	6
2003-163	−5.99°	154.76°	268°	*SKS*	6
2003-185	−5.47°	151.69°	270°	*SKS*	3
2003-203	−15.42°	166.14°	254°	*SKS*	7
2003-206	−1.53°	149.69°	275°	*SKS*	6
2003-208	−21.08°	−176.59°	238°	*SKS*	3
2003-273	−30.44°	−177.40°	232°	*SKS*	6

[a]BAZ, back azimuth.

area with well-constrained splits (Y14 and Y47) are close to parallel to plate motion. Stations northeast of Yellowstone (Y50 and Y51) have splitting fast directions (61°) parallel to plate motion, although null splits indicate a slightly more easterly oriented fast direction.

[24] East and southeast of Yellowstone, the splitting directions vary from NE to E-W. Station Y64 had nearly identical splitting parameters ($\phi = \sim 90°$, $\delta t = \sim 0.83$ s) for *SKS* and *SKKS* from the same event. One permanent station, BW06, did not have any high-quality splitting events during the five years (1999–2003) examined for the study, although it did have seven null splits from NW and WSW back azimuths. Station Y35 at the southeastern end of the array had two splits oriented roughly E-W similar to the most northern station in the temporary CD-ROM array [*Fox et al.*, 2001], which is <100 km SW of Y35.

[25] Most stations have just one high-quality split so interpretation in terms of complex models with multiple layers or dipping fast polarization directions is not possible. Station HLID is an exception. This permanent station recorded 9 high-quality split *S* waves from 1999 through 2003. The ϕ parameters computed at HLID demonstrate slight back-azimuthal dependence; split phases from events with SW back azimuths have WNW fast directions while split phases from the NW have E-W to WSW fast axes. The 2σ uncertainties on these measurements overlap so a more complex model is not required by the data. However, *Walker* [2004] showed that the pattern is consistent with an anisotropic layer with direction of fast anisotropy dipping gently to the west. It may also be consistent with a model in which two or more anisotropic layers are responsible for the splitting. On the other hand, *Hartog and Schwartz* [2001] show that the four parameters describing the anisotropic structure of two horizontal layers cannot be uniquely determined using apparent splitting parameters alone.

[26] Finally, the permanent station LKWY within the youngest Yellowstone caldera had anomalous splits with NW oriented fast axes and large split times in excess of 2.5 s. The single A quality split from LKWY is plotted in Figure 3. The waveforms and diagnostic plots used in the

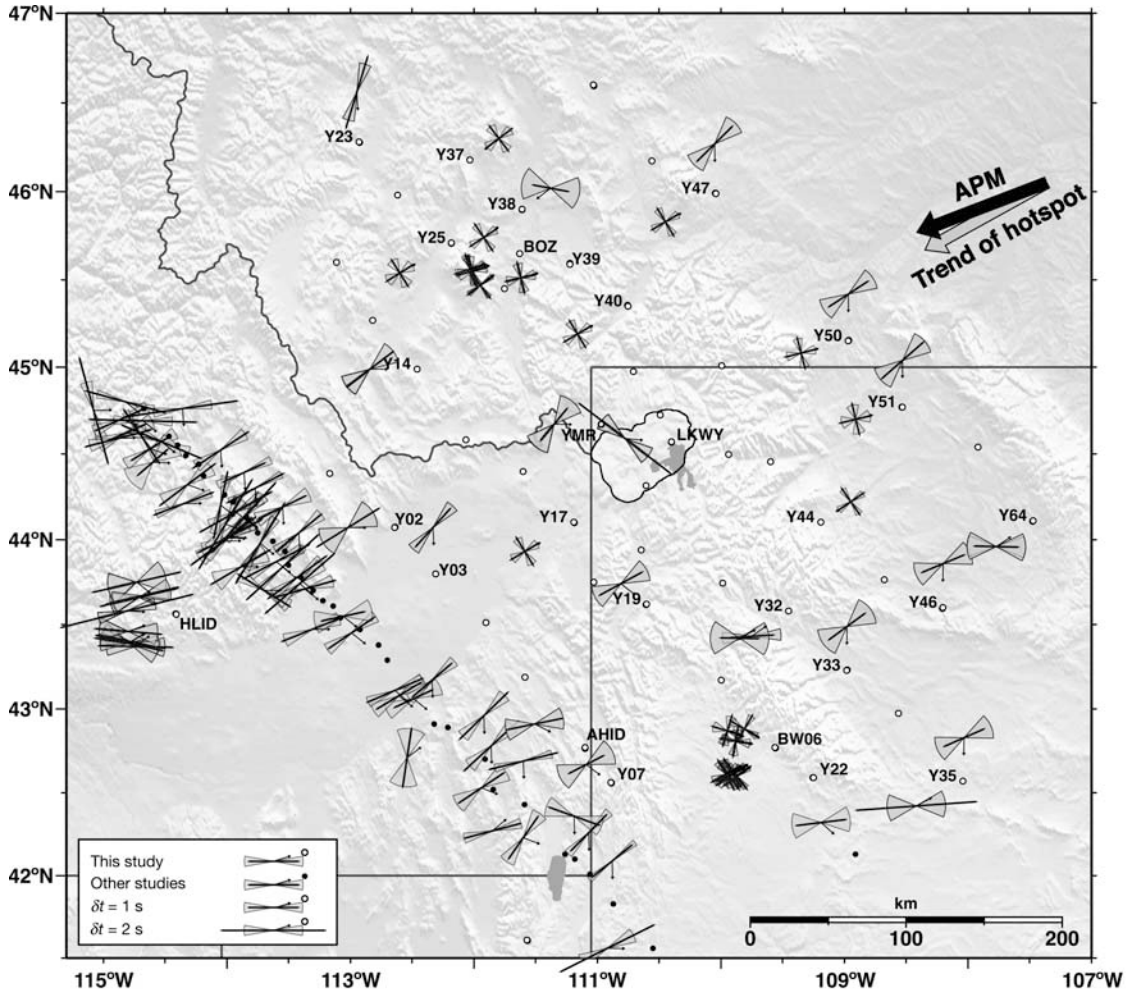

Figure 3. A quality individual event splitting parameters plotted as sticks aligned with the fast polarization direction with δt proportional to the length of the stick. Null splits are plotted with crosses. The sticks are plotted at the 150 km pierce points of the incoming ray to highlight any back-azimuthal dependence on the splitting parameters. Small arrows indicate the propagation direction. Open circles represent stations used in this study, and solid circles are from *Schutt et al.* [1998] and D. L. Schutt (unpublished data, 2003). Large arrows represent the direction of absolute plate motion and the trend of the Yellowstone hot spot from *Gripp and Gordon* [2002].

splitting analysis of this event are shown in Figure 4. This splitting measurement and two B quality measurements are at high angles to the direction of APM and ϕ at neighboring stations. This may indicate a strong, shallow source of anisotropy beneath the caldera.

3.3. Station Average Splitting Results

[27] Average splitting parameters for individual stations are especially useful at temporary stations for which there are few well-constrained splitting measurements. The results from several events are summed as described above to arrive at an average pair of splitting parameters for each station. A few caveats must be considered when interpreting station average splits, however. In general, station averaging of vertically propagating waves is only valid for a simple anisotropic medium with a horizontal fast polarization direction. This is a reasonable assumption in most areas, although features such as subducting slabs and ascending plumes may produce anisotropic fabric with dipping fast axes. Subhorizontal fast axes and multiple layers of anisotropy yield split parameters with back-azimuthal dependence. In addition, the phases used in the average must have very small angles of incidence. *SKS*, *SKKS*, and *PKS* phases used in this study have small incidence angles (<15°).

[28] Stations with strong back-azimuthal dependence may produce unrealistic station average splitting parameters, so care must be taken to examine the individual splitting results used in the average. For example, station Y23 has individual splits with both NNE and NNW ϕ, but station average $\phi = 58°$, and $\delta t = 0.35$ s. A few of the stations in this study have a back-azimuthal dependence, but only HLID has high-quality splitting results that exhibit back-azimuthal dependence. In general, the stations in this study have consistent splitting from all back azimuths and null splitting from events parallel or perpendicular to the fast direction computed by averaging.

[29] The station average splitting results for all the stations are plotted in Figure 5 along with the station

Table 2. Individual Event Splitting Parameters

					Silver and Chan [1991] Method				*Levin et al.* [1999] Method			
Year-Day[a]	Station	Phase	BAZ	S/N[b]	δt, s	$\delta t-2\sigma$,[c] s	ϕ	$\phi-2\sigma$[c]	δt, s	$\delta t-2\sigma$,[c] s	ϕ	$\phi-2\sigma$[c]
2001-184	AHID	*SKS*	296°	5.4	1.2	0.4	78.4°	21.5°	1.2	0.2	81.0°	9.4°
N2000-178	BOZ	*SKS*	253°	5.2	0.9	–	72.2°	17.5°	0.4	0.2	27.0°	9.5°
N2002-002	BOZ	*SKS*	251°	6.4	1.1	–	74.2°	22.1°	0.3	0.2	23.0°	12.3°
N2003-273	BOZ	*SKS*	232°	6.9	1.1	–	53.0°	11.2°	0.1	0.2	94.0°	12.2°
N2001-118	BW06	*SKS*	242°	10.9	0.7	–	61.1°	21.1°	0.1	0.2	113.0°	16.0°
N2001-185	BW06	*SKS*	239°	4.5	3.6	–	55.2°	21.5°	0.1	0.2	116.0°	13.9°
N2001-285	BW06	*SKS*	290°	5.7	1.2	–	16.7°	21.4°	0.5	0.2	73.0°	9.0°
N2002-181	BW06	*SKS*	241°	7.7	0.4	–	59.9°	12.8°	0.1	0.1	114.0°	9.3°
N2002-251	BW06	*SKS*	280°	9.5	1.0	–	9.7°	18.8°	0.0	0.1	154.0°	13.0°
N2003-124	BW06	*SKS*	234°	5.4	0.9	–	53.2°	13.5°	0.3	0.4	111.0°	15.9°
N2003-146	BW06	*SKS*	302°	12.8	0.5	–	30.3°	14.6°	0.1	0.1	87.0°	7.4°
2000-228	DUG	*SKS*	232°	8.0	1.6	0.4	161.9°	12.6°	1.6	0.1	156.0°	5.1°
2003-146	DUG	*SKS*	298°	6.1	1.5	0.3	153.3°	15.0°	1.5	0.3	150.0°	12.4°
1999-169	HLID	*SKS*	295°	5.5	1.8	0.4	76.9°	19.9°	1.8	0.1	88.0°	6.5°
1999-200	HLID	*SKS*	232°	5.5	1.6	0.4	91.2°	18.9°	1.6	0.2	103.0°	9.8°
2001-255	HLID	*SKS*	238°	4.4	1.5	0.5	103.0°	28.2°	1.5	0.2	111.0°	11.2°
2002-085	HLID	*SKS*	308°	5.7	2.0	0.8	76.9°	31.2°	2.0	0.2	87.0°	7.7°
2002-181	HLID	*SKS*	238°	11.7	1.4	0.2	102.0°	13.2°	1.4	0.1	111.0°	7.2°
2002-231	HLID	*SKS*	238°	10.5	1.5	0.3	98.3°	13.1°	1.5	0.1	104.0°	6.4°
2002-133	HLID	*SKS*	249°	7.3	1.4	0.8	94.9°	21.4°	1.0	0.3	113.0°	13.3°
2003-146	HLID	*SKS*	298°	14.8	1.7	0.4	76.5°	20.9°	1.7	0.1	84.0°	5.0°
2003-206	HLID	*SKS*	273°	5.7	3.2	0.5	75.8°	11.4°	3.3	0.1	87.0°	2.8°
2003-206	LKWY	*SKS*	276°	5.5	2.7	0.8	127.6°	18.4°	2.7	0.6	123.0°	13.1°
2003-158	YMR	*SKS*	271°	7.8	0.8	0.3	39.5°	26.8°	0.7	0.1	45.0°	8.7°
2000-356	Y02	*SKS*	270°	3.5	1.6	0.9	58.0°	29.7°	1.8	0.2	63.0°	8.0°
2000-199	Y03	*SKS*	357°	7.0	1.0	0.2	42.2°	12.8°	1.1	0.1	37.0°	5.8°
2000-299	Y07	*PKS*	308°	19.6	0.7	0.6	62.7°	26.4°	0.4	0.1	86.0°	11.3°
2000-356	Y14	*SKS*	270°	3.6	1.2	0.4	52.7°	23.2°	1.2	0.1	56.0°	5.2°
N2001-118	Y17	*SKS*	240°	8.0	1.1	–	58.8°	18.6°	0.1	0.1	107.0°	12.5°
2000-299	Y19	*PKS*	309°	6.2	1.0	0.8	61.3°	22.5°	1.0	0.2	76.0°	7.7°
2000-199	Y23	*SKS*	357°	8.7	1.7	0.6	16.9°	11.8°	1.7	0.2	7.0°	6.0°
N2001-118	Y25	*SKS*	240°	5.6	1.1	–	57.8°	23.9°	0.2	0.1	18.0°	8.9°
2000-228	Y32	*SKS*	235°	5.7	0.9	0.2	86.4°	11.5°	0.8	0.1	100.0°	6.1°
2001-118	Y32	*SKS*	242°	13.0	0.7	0.6	91.2°	33.4°	0.5	0.2	111.0°	14.4°
2000-199	Y33	*SKS*	0°	5.4	0.9	0.5	53.7°	29.9°	0.9	0.2	50.0°	13.2°
2000-199	Y35	*SKS*	1°	11.0	0.8	0.6	66.2°	24.7°	0.8	0.1	77.0°	6.9°
2001-139	Y35	*SKS*	242°	2.7	2.8	0.9	85.9°	26.4°	2.9	0.3	85.0°	14.4°
N2000-276	Y37	*PKS*	52°	6.2	1.0	–	52.9°	20.5°	0.3	0.1	102.0°	17.3°
N2000-228	Y38	*SKS*	234°	8.2	1.2	–	56.4°	17.0°	0.1	0.1	108.0°	18.5°
2000-276	Y38	*PKS*	52°	8.8	0.6	0.3	100.6°	32.1°	0.6	0.1	90.0°	12.5°
N2000-178	Y39	*SKS*	254°	5.0	1.3	–	76.6°	20.1°	0.3	0.2	31.0°	9.4°
N2001-118	Y40	*SKS*	241°	7.8	1.2	–	59.2°	19.0°	0.0	0.1	23.0°	8.4°
N2000-276	Y44	*PKS*	56°	12.5	0.3	–	55.5°	13.7°	0.1	0.0	16.0°	13.7°
2000-199	Y46	*SKS*	1°	8.6	0.9	0.6	67.3°	24.1°	0.8	0.2	56.0°	8.6°
2000-199	Y47	*SKS*	359°	6.3	1.0	0.3	45.2°	21.9°	1.0	0.1	42.0°	9.3°
N2001-118	Y47	*SKS*	241°	10.6	1.2	–	59.3°	16.1°	0.1	0.1	25.0°	9.2°
2000-199	Y50	*SKS*	0°	5.5	0.9	0.4	56.7°	21.8°	0.9	0.1	56.0°	8.9°
N2001-009	Y50	*SKS*	255°	5.2	1.1	–	75.7°	18.0°	0.2	0.3	126.0°	12.5°
N2000-178	Y51	*SKS*	255°	4.9	1.3	1.8	76.4°	24.5°	0.2	0.4	127.0°	15.3°
2000-199	Y51	*SKS*	0°	6.3	1.2	0.4	48.6°	24.7°	1.2	0.2	60.0°	10.9°
2000-228	Y64	*SKS*	236°	11.6	0.8	0.3	91.2°	21.0°	0.9	0.2	89.0°	9.9°
2000-228	Y64	*SKKS*	236°	8.3	0.8	0.4	91.6°	27.5°	0.8	0.2	97.0°	12.8°

[a]Prefix N indicates null split.
[b]S/N is signal to noise ratio.
[c]The 2σ indicates uncertainty at 95% confidence interval; dash indicates uncertainties that are larger than the search area.

averages from *Schutt et al.* [1998]. Symbols are as in Figure 3 except the sticks are plotted at the station locations instead of at the 150 km pierce points. The average splitting parameters are also plotted as a function of longitude in Figure 6 to facilitate interpretation. Table 3 lists the station average splitting parameters.

[30] Station average delay times are between 0.5 and 1.25 s over most of the array. Many of the stations with small station average δt (<0.5 s) have individual splits that exhibit back-azimuthal dependence (HWUT, Y13, Y20, Y23, Y24, Y33, Y38, Y39, Y43, Y44 in Figures 3 and 5) possibly indicating a complex anisotropic structure below the stations inappropriate for analysis with station averages. These stations are noted in Figures 3 and 5. The largest average split times over 2 s are at stations within the Yellowstone caldera: Y100 and Y102.

[31] Station average ϕ cluster around the direction of APM (249.5° ± 10.7°) and the trend of the Yellowstone hot spot track (241.0° ± 23.8°) as do the station average ϕ from *Schutt et al.* [1998]. Stations with large deviations from these directions (HLID, LKWY, Y20, Y22, Y33, Y34, Y35, Y40, Y61, Y64, Y100 in Figures 3 and 5) are far from

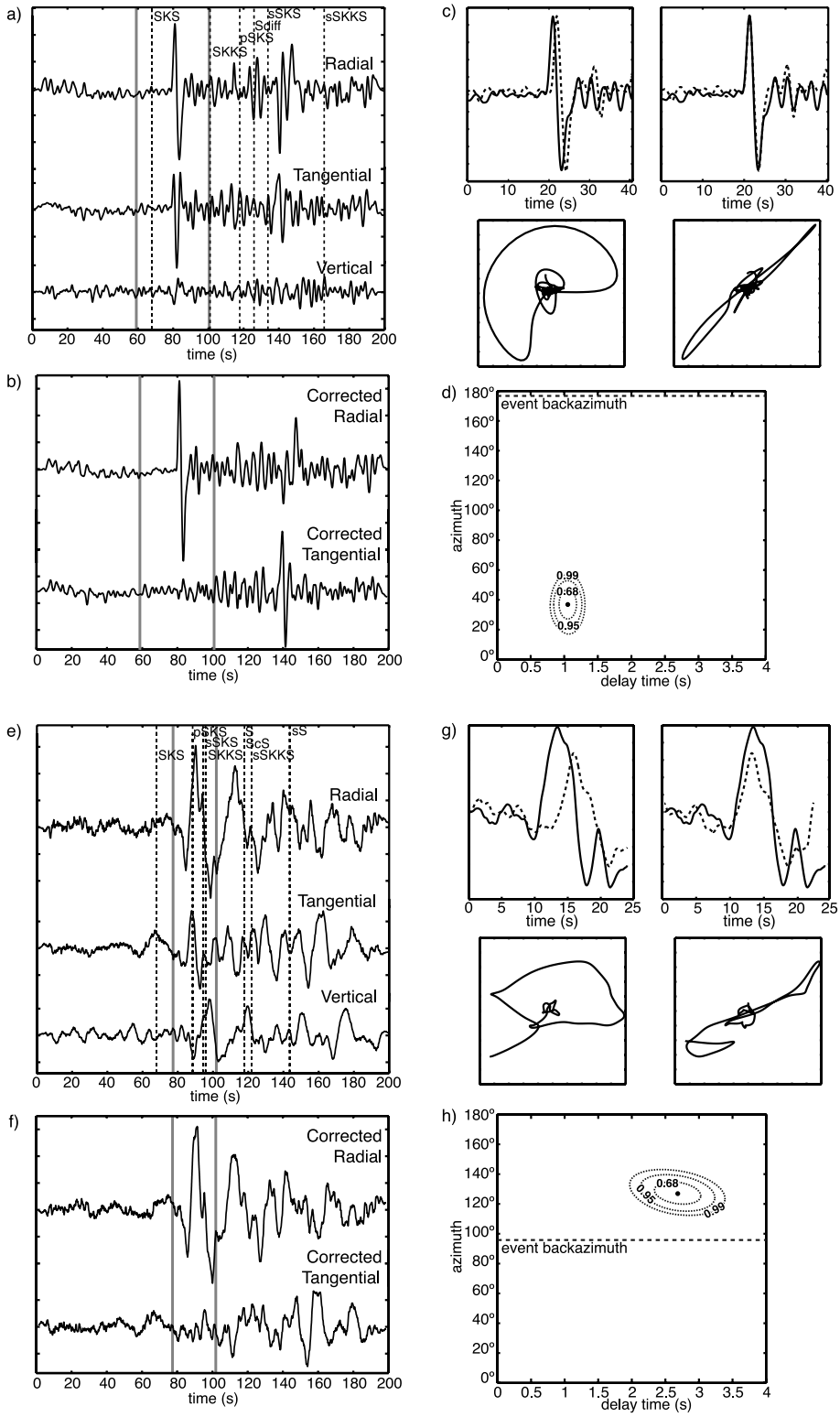

Figure 4. Example A quality shear wave splitting measurements at station Y03 (Figures 4a–4d) on the ESRP and LKWY in the Yellowstone caldera (Figures 4e–4h): (a and e) the original band-pass-filtered radial, tangential, and vertical traces with predicted travel times (dashed lines) and time interval used to estimate splitting (gray lines) marked; (b and f) the filtered radial and tangential waveforms after correcting for the apparent splitting; (c and g) (top) fast and slow waveforms and (bottom) corresponding particle motions in the window used to estimate the splitting (left) before and (right) after correction for split delay; (d and h) the minimum corrected energy on the tangential component (dot) and contours showing the confidence ellipsoids for different confidence intervals estimated with the method of *Silver and Chan* [1991]. Note that these waveforms are not from the same event.

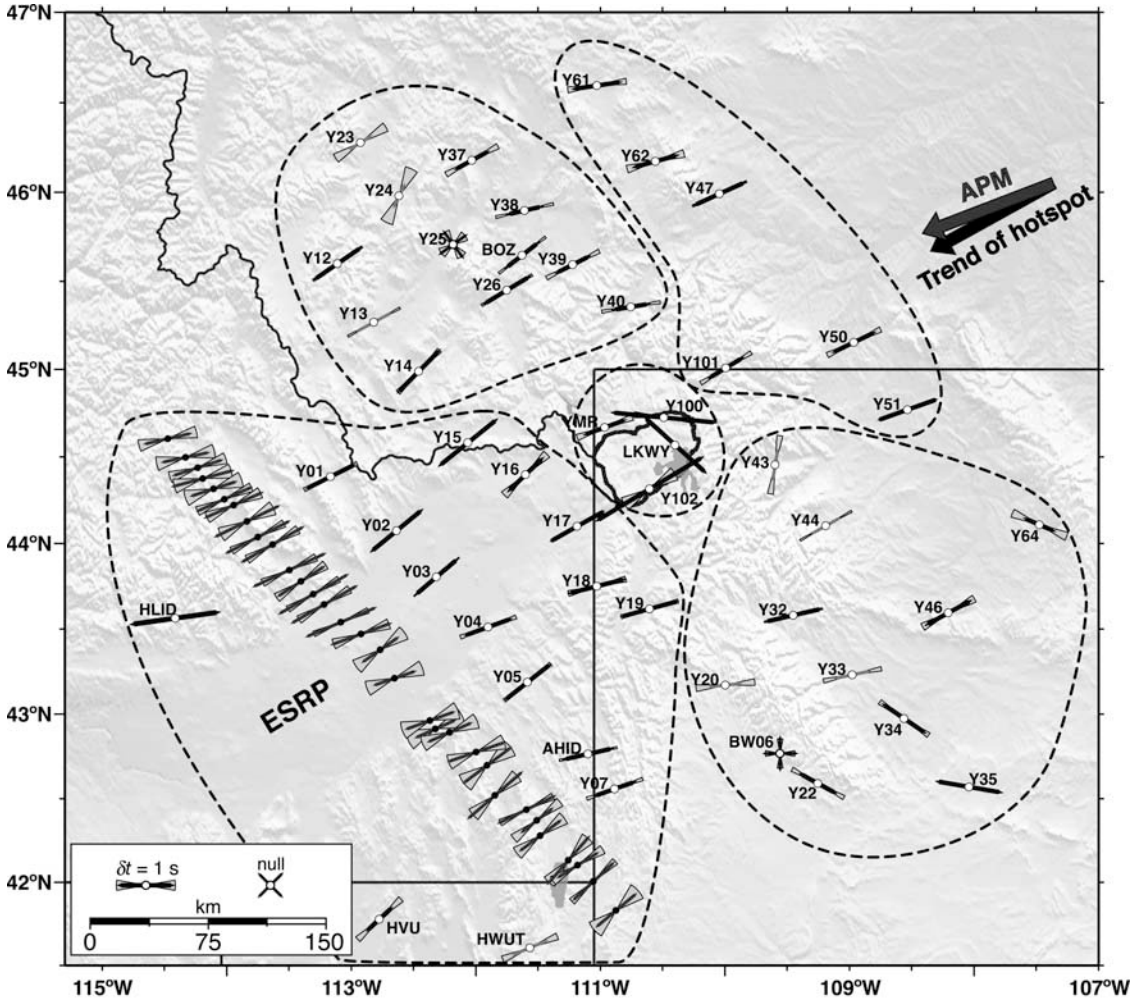

Figure 5. Station average splitting parameters plotted as sticks parallel to ϕ. Length of sticks are proportional to δt. Circles represent station locations with white circles from this study, and solid circles from *Schutt et al.* [1998]. Light sticks are for stations with demonstrated back-azimuthal dependence in individual splitting parameters. Large arrows represent the direction of absolute plate motion and the trend of the Yellowstone hot spot from *Gripp and Gordon* [2002]. Note that station averages are computed from more data than are shown in Figure 3.

the ESRP, have individual ϕ that show back-azimuthal dependence, or are within the Yellowstone caldera.

4. Discussion of Shear Wave Splitting Measurements

[32] The shear wave splitting results from this study imply a relatively simple anisotropic structure beneath much of the region surrounding the Yellowstone hot spot. Figure 7 shows splitting results from stations across the western United States. The plot combines individual splits and station average data from several studies and previous compilations [*Silver*, 1996; *Schutt et al.*, 1998; *Savage and Sheehan*, 2000; *Polet and Kanamori*, 2002; *Walker*, 2004; D. L. Schutt, unpublished data, 2003]. The similarity in splitting directions at Yellowstone and across the ESRP is remarkable in this western U.S. context. The upper mantle fabric under Yellowstone seems relatively simple and can broadly be interpreted as due to North America plate motion. The shear of the North America plate over the relatively stable mantle would produce a lattice-preferred orientation (LPO) of olivine fast *a* axes, and therefore ϕ, in the direction of plate motion. The mean station average δt of 0.9 s is explained by a 100-km-thick layer of 4% anisotropic mantle. This simple asthenospheric flow model has been invoked to explain teleseismic shear wave splitting observations worldwide.

[33] Although asthenosphere flow is an attractive model for the observed splitting parameters at Yellowstone, the stations with splitting fast axes that deviate from the APM require an alternate explanation. Archean lithosphere fabric and melt-filled cracks may produce detectable anisotropy in some areas. Small-scale convection in the upper mantle may also produce anisotropic fabric with fast polarization directions that differ from the APM.

[34] In the following five subsections, splitting results from this study will be discussed for different parts of the array. The discussion begins with an interpretation of the ESRP splits, then moves clockwise around the Yellowstone caldera to stations north, NE, east and SE of Yellowstone.

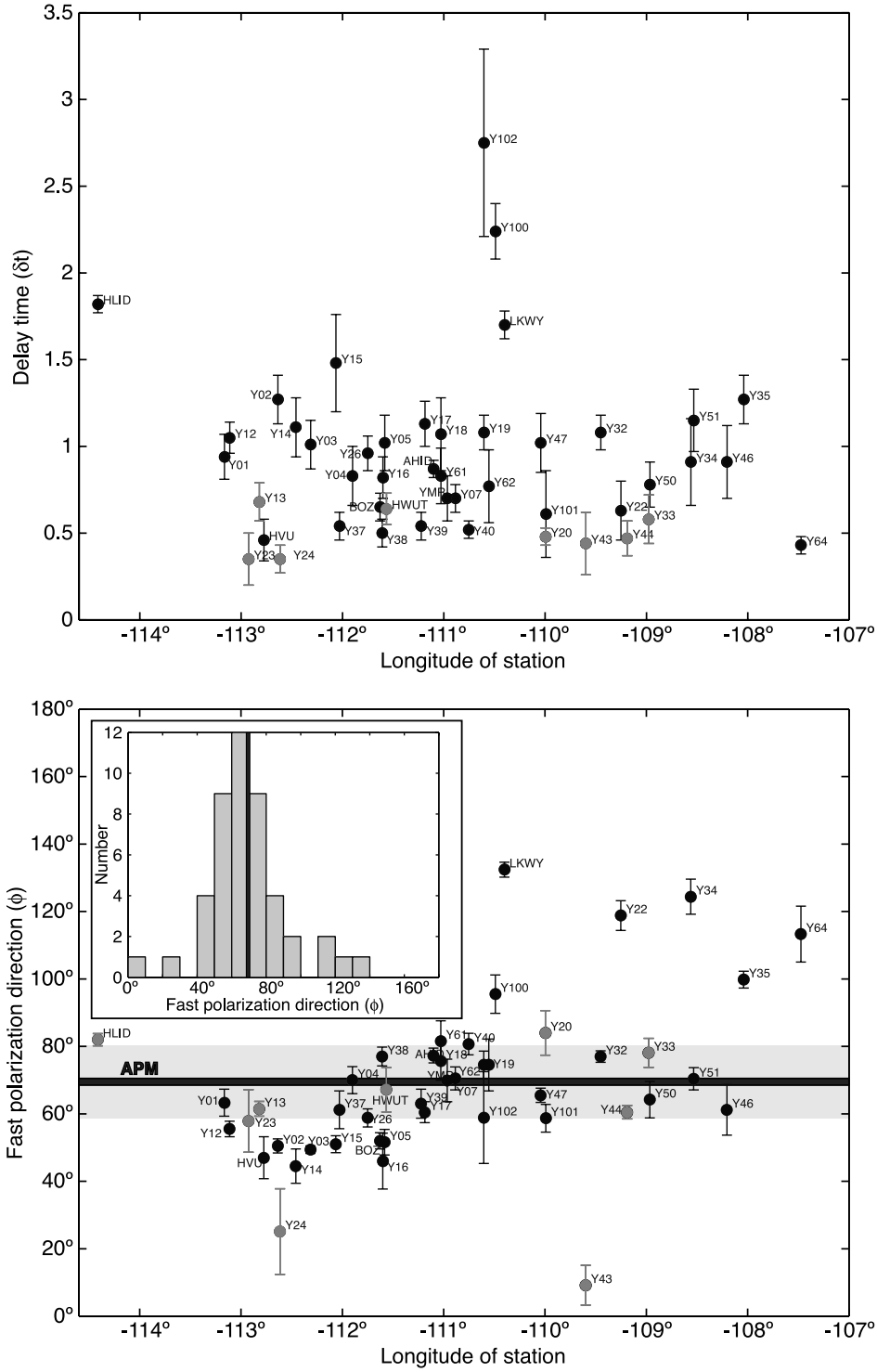

Figure 6. Station average splitting parameters plotted as a function of station longitude. Light symbols are for stations with demonstrated back-azimuthal dependence in individual splitting parameters. The dark line indicates the direction of APM. Inset shows histogram of fast polarization directions.

Finally, the unusual splits for stations within the caldera are discussed. These five areas are circled in Figure 5 to simplify the discussion. Larger-scale interpretations are made in the last two subsections of the discussion. The pattern of splitting that might be expected for plume-influenced flow at the base of the lithosphere is modeled and compared to the station average splits. The last subsection details implications of eastward mantle flow beneath the array.

4.1. Shear Wave Splitting on and Adjacent to the Eastern Snake River Plain

[35] *Schutt and Humphreys* [2001] interpret the uniform southwesterly trend of fast axes across the ESRP as result-

Table 3. Station Average Shear Wave Splitting Parameters

Station	Latitude	Longitude	δt (s)	δt-2σ (s)	ϕ	ϕ-2σ
Y01	44.39°	−113.17°	0.9	0.1	63.3°	4.0°
Y02	44.07°	−112.64°	1.3	0.1	50.5°	2.1°
Y03	43.81°	−112.31°	1.0	0.1	49.4°	1.1°
Y04	43.51°	−111.90°	0.8	0.2	70.0°	4.0°
Y05	43.19°	−111.58°	1.0	0.2	51.6°	3.8°
Y07	42.56°	−110.89°	0.7	0.1	70.5°	3.4°
Y100	44.72°	−110.49°	2.2	0.2	95.5°	5.7°
Y101	45.01°	−109.99°	0.6	0.3	58.7°	4.1°
Y102	44.32°	−110.60°	2.8	0.5	58.9°	13.6°
Y12	45.60°	−113.11°	1.1	0.1	55.5°	2.3°
Y13	45.27°	−112.82°	0.7	0.1	61.5°	2.2°
Y14	44.99°	−112.46°	1.1	0.2	44.5°	5.1°
Y15	44.58°	−112.06°	1.5	0.3	51.0°	2.5°
Y16	44.40°	−111.60°	0.8	0.1	46.0°	8.3°
Y17	44.10°	−111.19°	1.1	0.1	60.5°	3.1°
Y18	43.75°	−111.03°	1.1	0.2	75.7°	5.7°
Y19	43.62°	−110.60°	1.1	0.1	74.5°	4.1°
Y20	43.17°	−110.00°	0.5	0.1	84.0°	6.6°
Y22	42.59°	−109.25°	0.6	0.2	118.8°	4.4°
Y23	46.28°	−112.93°	0.4	0.2	57.9°	9.3°
Y24	45.98°	−112.62°	0.4	0.1	25.1°	12.7°
Y26	45.45°	−111.75°	1.0	0.1	58.8°	2.7°
Y32	43.58°	−109.45°	1.1	0.1	77.0°	1.7°
Y33	43.23°	−108.98°	0.6	0.1	78.1°	4.3°
Y34	42.97°	−108.56°	0.9	0.3	124.4°	5.2°
Y35	42.57°	−108.04°	1.3	0.1	99.8°	2.5°
Y37	46.18°	−112.03°	0.5	0.1	61.2°	5.6°
Y38	45.90°	−111.61°	0.5	0.1	77.0°	2.8°
Y39	45.59°	−111.22°	0.5	0.1	63.0°	4.3°
Y40	45.35°	−110.75°	0.5	0.1	80.7°	3.2°
Y43	44.45°	−109.60°	0.4	0.2	9.2°	5.9°
Y44	44.10°	−109.19°	0.5	0.1	60.5°	2.0°
Y46	43.60°	−108.20°	0.9	0.2	61.2°	7.5°
Y47	45.99°	−110.04°	1.0	0.2	65.5°	2.1°
Y50	45.15°	−108.97°	0.8	0.1	64.2°	5.4°
Y51	44.77°	−108.53°	1.2	0.2	70.4°	3.3°
Y61	46.60°	−111.03°	0.8	0.2	81.6°	6.0°
Y62	46.17°	−110.56°	0.8	0.2	74.5°	7.7°
Y64	44.11°	−107.47°	0.4	0.1	113.3°	8.3°
AHID	42.77°	−111.10°	0.9	0.1	77.3°	2.2°
BOZ	45.65°	−111.63°	0.7	0.1	52.0°	2.4°
DUG	40.20°	−112.81°	0.8	0.1	164.7°	1.9°
HLID	43.56°	−114.41°	1.8	0.1	82.0°	1.8°
HVU	41.78°	−112.78°	0.5	0.1	47.0°	6.2°
HWUT	41.61°	−111.57°	0.6	0.1	67.2°	6.6°
LKWY	44.57°	−110.40°	1.7	0.1	132.4°	2.2°
YMR	44.67°	−110.97°	0.7	0.1	69.9°	6.3°

ing from relatively shallow asthenospheric flow. This agrees with the fast *Pn* anisotropy direction, which reflects uppermost mantle fabric. *Smith and Ekström* [1999] found the fast *Pn* direction is parallel to APM in the ESRP. The splitting results from stations on and adjacent to the ESRP in this study are mostly consistent with this interpretation. The combination of consistent splitting fast directions for events with different back azimuths and null splits for events with back azimuths parallel or perpendicular to the fast direction are explained with a single anisotropic layer.

[36] Shear wave splitting directions at stations farther from Yellowstone along the ESRP are not consistent with those of *Schutt et al.* [1998] or this study. Results from *Walker*'s [2004] temporary four-station array hint at a rotation in fast anisotropy directions from NE-SW to E-W and ESE-WNW where the ESRP becomes oriented NW-SE. The GPS-derived velocity field relative to stable North America appears to mimic this rotation as well, however the rate of extension on the ESRP (∼2 mm/yr) [*Puskas et al.*, 2002] is roughly an order of magnitude lower than the plate motion of 2.6 cm/yr [*Gripp and Gordon*, 2002] and may be relatively insignificant.

4.2. Splitting at Stations North of Yellowstone

[37] Splitting fast axes at stations north of Yellowstone (BOZ, Y12, Y13, Y14, Y23, Y24, Y25, Y26, Y37, Y38, Y39, Y40 in Figures 3 and 5) can also be explained by simple asthenosphere flow, although the delay times are generally small ($\delta t < 0.5$ s). Unlike stations on the ESRP, split waveforms are noisy and few stations have any high-quality splits. The two stations that do have high-quality splits (Y23, Y24) have fast polarization directions that are significantly different from the station averages. Asthenospheric flow may produce splitting parallel to APM, but propagation of the split waves through the complex structure in the lithosphere beneath these stations likely scatters energy.

4.3. Splitting at Stations NE of Yellowstone

[38] Splitting fast directions at stations NE of Yellowstone (Y47, Y50, Y51, Y61, Y62, and Y101 in Figures 3 and 5) are also parallel to the direction of plate motion. Again, the simplest explanation for this orientation is simple asthenosphere flow. However, the LPO in the asthenosphere may be complemented by similarly oriented anisotropic structure in the lithosphere. Several Precambrian provinces strike NE, parallel to the direction of plate motion, and may be affecting the splitting results (Figure 8). For example, the Proterozoic Madison mylonite zone may represent an ancient, deep shear zone [*Erslev and Sutter*, 1990]. Anisotropic fabric that would have developed while that feature was active would have a fast direction approximately parallel to the shear direction causing an additive effect in the delay between shear waves split in the underlying asthenosphere. Station Y47 which is closest to the Madison shear zone has $\delta t = 1.0$ s, which is not especially large, but larger than the split times of the rest of the stations north of Yellowstone.

4.4. Splitting at Stations East and SE of Yellowstone

[39] The pattern of splitting fast directions east and SE of Yellowstone is quite complex with several stations having ϕ far from the plate motion direction. Here, we suggest that lithosphere structure influences the observed shear wave splitting. For example, a north dipping *P* and *S* wave high-velocity anomaly imaged with tomography extends from the surface expression of the Cheyenne belt to a depth of 200 km [*Dueker et al.*, 2001]. *Dueker et al.* [2001] interpret it as an old slab associated with suturing along the Cheyenne belt. The thermal signature of this remnant slab would be diffused, so the seismic anomaly is attributed to anisotropic structure in the slab. A change in the shear wave splitting fast directions was observed in two arrays that cross the suture and could be due to a north dipping fast axis [*Fox et al.*, 2001].

[40] The station averages as well as the poorly constrained individual splitting measurements at Y34 and Y22 are consistent with a NW dipping fast axis (Figures 3 and 5). Although Y34 and Y22 are ∼150 km north of the surface expression of the Cheyenne Belt, they sit above a

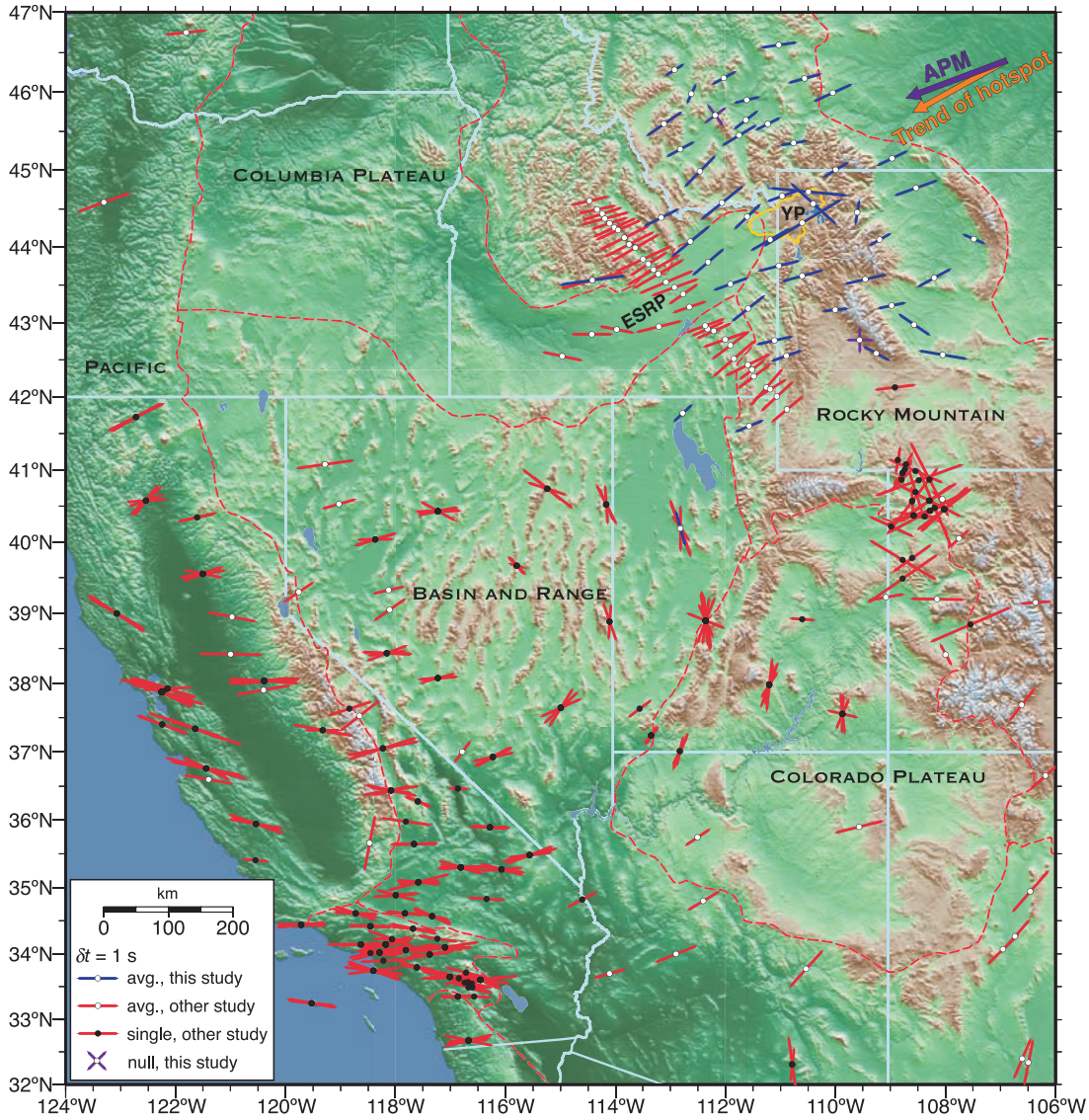

Figure 7. Splitting parameters across the western United States plotted as in previous figures. Station averages are open circles; individual event splits are solid circles. Data from this study (blue) were combined with data from other researchers (red) [*Silver*, 1996; *Schutt et al.*, 1998; *Savage and Sheehan*, 2000; *Polet and Kanamori*, 2002; *Walker*, 2004; D. L. Schutt, personal communication, 2003]. State (light green) and physiographic (dashed red) boundaries are shown for reference. The orange line outlines the three Yellowstone Plateau (YP) calderas.

NW dipping high-velocity anomaly [*Waite et al.*, 2003]. This anomaly may be similar to the feature found by *Dueker et al.* [2001]. The splits measured above the anomaly could be due to a dipping anisotropic structure rather than asthenosphere flow.

[41] East of Yellowstone the fast *Pn* direction is E-W [*Smith and Ekström*, 1999]. The easternmost stations in the array (Y35, Y46, Y64) have varied fast polarization directions that are difficult to interpret. They may be related to deep lithospheric structural features in the Archean Wyoming block, but such interpretation is conjectural.

4.5. Splitting at Yellowstone Caldera Stations

[42] The most striking feature of Figure 5 is the rotation of fast polarization directions at stations in the Yellowstone caldera. The large change in direction (73° between Y102 and LKWY; 62° between YMR and LKWY) over such small distances (~30 km) suggests a shallow source. However, splitting at stations LKWY, Y100 and Y102 also have the largest average delay times ($\delta t > 2$ s) of the stations in the array. The large split times and shallow source require a highly anisotropic medium.

[43] Fresnel zones have been used to estimate the depth of the anisotropy measured with teleseismic shear wave splitting [e.g., *Alsina and Snieder*, 1995; *Rümpker and Ryberg*, 2000]. The width of the Fresnel zone depends on the wavelength and path length of the ray. If the Fresnel zones of two waves traveling in the same direction overlap, the waves should have similar characteristics. Consider two stations that record an *SKS* from the same earthquake. Near

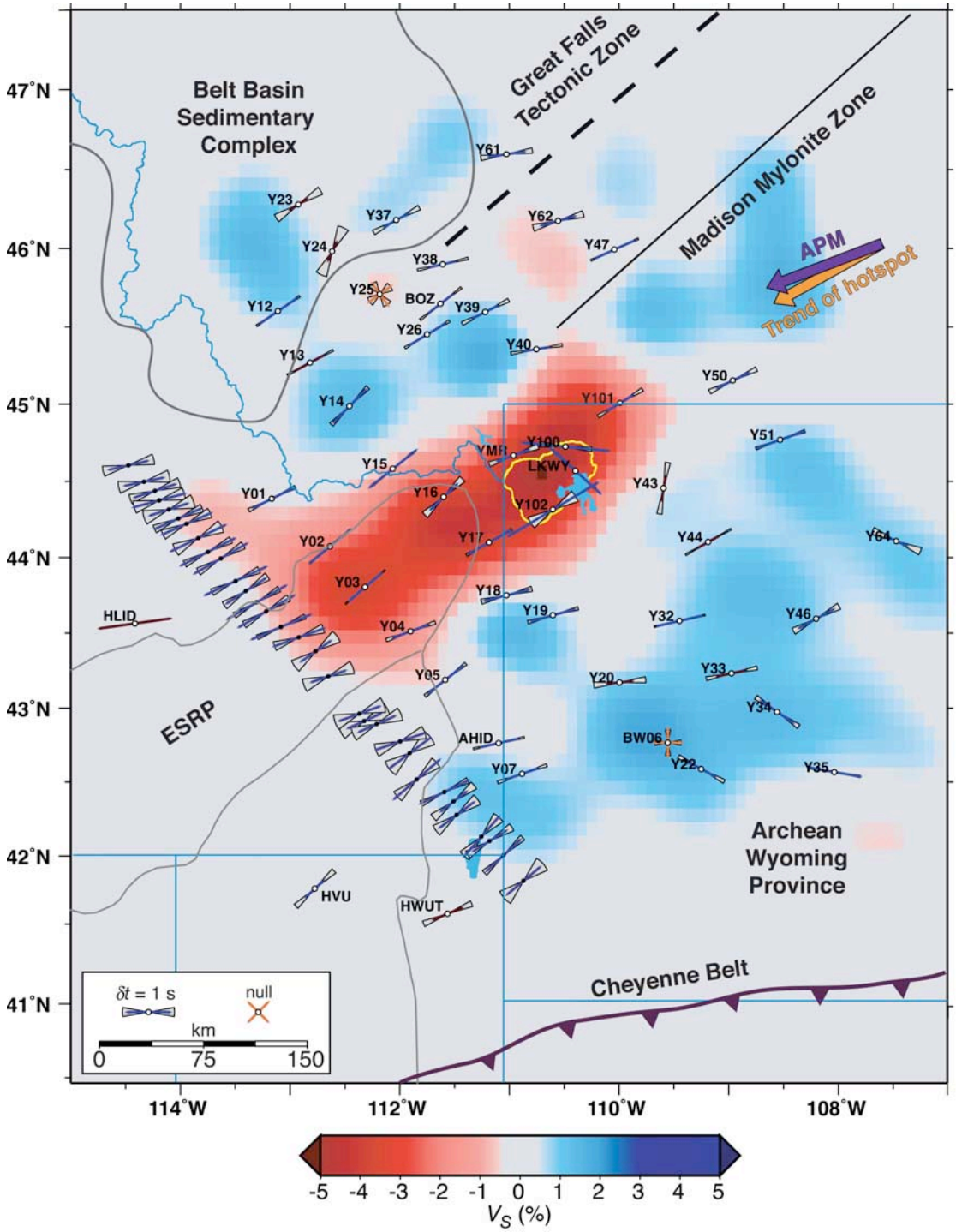

Figure 8. Station averages plotted over a slice through the shear wave velocity model at 90 km depth [*Waite et al.*, 2003]. Major Precambrian structural features are plotted after *Karlstrom et al.* [2002]. The high-velocity (blue) anomaly in the SE of the array may represent an Archean structural feature.

the source, the ray paths are nearly the same so the waves should be the same. The ray paths diverge as they approach the recording station, and their Fresnel zones overlap less. The Fresnel zones also get smaller near the stations. At shallow depths below the stations, the Fresnel zones may no longer overlap, so the waves will sense different medium characteristics. The depth at which the Fresnel zones separate depends on the station spacing and the width of the Fresnel zones.

[44] *Rümpker and Ryberg* [2000] estimate the sensitivity range (roughly equivalent to Fresnel zone) of vertically propagating shear waves using finite difference modeling. The model consists of a 150-km-thick anisotropic layer that is moved from the surface through the upper mantle. This

modeling suggests *S* waves with a dominant period of 8 s are sensitive to changes in anisotropy to a distance of at least 75 km from the station. This distance increases with depth to the top of the anisotropic layer. *Rümpker and Ryberg* [2000] do not vary the thickness of the anisotropic layer. For a given layer depth, the sensitivity distance will decrease with a thinner anisotropic layer. *Alsina and Snieder* [1995] used a simpler modeling technique to estimate the sensitivity range of *S* waves that does not account for thickness of the anisotropic layer. This modeling yields much smaller estimates for the sensitivity range for a given depth of the top of the anisotropic layer ($\sim$40 km smaller than estimated by *Rümpker and Ryberg* [2000]).

[45] Waves that sense two adjacent anisotropic layers can produce apparent splitting unlike what would be caused by either layer alone [e.g., *Rümpker and Ryberg*, 2000]. Therefore two closely spaced stations with significantly different splitting parameters, such as Y102 and LKWY, must be interpreted with caution. The sensitivity ranges of stations Y102 and LKWY, which are 30 km apart, may overlap at all depths. Splitting results from station LKWY do not indicate significant variation with back azimuth or dominant period as would be expected for vertically or laterally varying anisotropy. However, a wider range of back azimuths might reveal some variation in the splitting parameters. There were no good events recorded from eastern back azimuths at LKWY (i.e., all useable split waves had back azimuths from 180° to 360°). The station average ϕ at Y102 is not as well constrained and may result from a complex anisotropic structure. Despite the possible complications in the interpretation, there is certainly strong anisotropy in the lithosphere beneath Yellowstone.

[46] Stress-oriented parallel fluid-filled cracks may cause the anomalous splitting observed in the Yellowstone caldera. Because the scale of these cracks is much smaller than the wavelengths of teleseismic shear waves, the result is an anisotropic structure with the slow direction parallel to the extension direction and the faster shear wave polarized parallel to the crack faces [e.g., *Kendall*, 1994]. Many authors have invoked aligned, fluid-filled microcracks to explain anisotropy in the lithosphere [see, e.g., *Gao et al.*, 1997; *Crampin and Chastin*, 2003, and references therein].

[47] The directions of maximum extensional strain (ε_{max}) estimated from GPS measurements [*Puskas et al.*, 2002], and minimum principal stress (σ_3) estimated from focal mechanisms [*Waite and Smith*, 2004] at Yellowstone support this interpretation of stress-induced crack opening. The directions of ε_{max} and σ_3 rotate from roughly N-S NW of the Yellowstone caldera to NE-SW within the central part of the caldera (e.g., near LKWY). This could produce crack anisotropy with a fast horizontal polarization direction NW-SE, which is parallel to the ϕ at LKWY (132° ± 2.2°). A similar model is proposed for the average ϕ at station Y100. *Waite and Smith* [2004] did not calculate the stress field around Y100 as there are few earthquakes in that area, but it is likely to be consistent with the rotation observed west of that area.

[48] Local earthquake tomography revealed an area of low V_P and low V_P/V_S in the shallow crust at Yellowstone interpreted as gas-filled pores [*Husen et al.*, 2004]. Gas-filled aligned microcracks could produce strong anisotropy in the upper crust. An analysis of local earthquake *S* wave splitting indicates anisotropy up to 5% in the upper crust [*Waite et al.*, 2004] that is likely due to stress-oriented microcracks. However, gas is likely confined to the shallow crust. A much thicker package of anisotropic material is required to explain the split times observed in the teleseismic data.

[49] The strong low-velocity anomaly in the upper mantle directly beneath Yellowstone caldera may be due, in part, to a small percentage of melt. The melt is likely organized in thin lenses oriented by the stress field [e.g., *Faul et al.*, 1994; *Hammond and Humphreys*, 2000]. Recently, *Kendall et al.* [2005] suggested rift-parallel splitting of $\sim$1.5 s observed above the Ethiopian rift is dominantly due to alignment of less than 0.1% melt fraction in the upper 70–90 km. This assumes a crack aspect ratio of 0.03. The larger split times observed within the Yellowstone caldera would require a larger melt fraction, thicker region of anisotropic material, cracks with a smaller aspect ratio, or a combination.

[50] Assuming a mean velocity of 4.3 km/s (4.5 km/s, −5%) from the tomography, anisotropy should be at least 8% to produce >2 s delays in a layer $\sim$100 km thick. The fast and slow shear wave velocities can be estimated using

$$\mathrm{K} = 100(V_1 - V_2)/(V) \quad (1)$$

where V_1 and V_2 are the fast and slow velocities and V is the mean velocity. The shear wave velocity in the fast direction would be 4.47 km/s, and the slow velocity would be 4.13 km/s to produce an anisotropy of 8%. If the anisotropy were due to oriented melt lenses and assuming that the fast shear waves are not affected by the melt pockets, $\sim$1% partial melt-filled cracks with a aspect ratio of 0.05 [*Hammond and Humphreys*, 2000] would reduce the velocity of slow waves by 7.7%. Our estimate is consistent with effective medium theory modeling used by *Ayele et al.* [2004] for 1% melt fraction and a crack aspect ratio of $\sim$0.025. A thinner anisotropic layer would require a higher percentage of partial melt-filled cracks or a smaller crack aspect ratio to produce the observed splitting.

[51] Station average fast polarization directions at Y102 and YMR are parallel to the plate motion direction. These measurements may be due to simple asthenosphere flow in the upper asthenosphere or stress-oriented cracks aligned parallel to the fast splitting directions at those stations. However, observations of ε_{max} and σ_3 do not support interpretation of stress-aligned cracks. The largest station average delay time of 2.8 s was computed for Y102. The station average δt at YMR is 0.7 s; however, individual splits at YMR indicate a degree of back azimuthal dependence that can result in smaller station average split times. Flow in the asthenosphere beneath the caldera could be influenced by upwelling material. The V_P and V_S tomography indicates low velocities to $\sim$200 km depth beneath the caldera and to $\sim$400 km depth 100 km NW of the caldera. If this low-velocity zone represents relatively warm, rising material, flow at the base of the plate could be turbulent to produce no coherent anisotropy.

[52] Laboratory measurements show that the presence of water in olivine can alter the development of LPO such that *a* axes are not parallel to the shear direction [*Jung and Karato*, 2001]. However, the tomography results indicate

melt is likely in the uppermost mantle and crust beneath Yellowstone [*Waite et al.*, 2003; *Husen et al.*, 2004; *Jordan et al.*, 2004]. Since water is preferentially segregated into the melt, free water is not likely to be present along with melt. Recent laboratory simulations show that melt can also influence the development of LPO via strain partioning, causing *a* axes to be oriented up to 90° to the shear direction [*Holtzman et al.*, 2003]. This implies that if the direction of maximum shear is parallel to plate motion and melt is present, LPO could develop with horizontal *a* axes oriented 90° to plate motion. Strain partitioning may influence the splitting fast directions at Yellowstone. At the least, this laboratory work highlights the complexity of interpreting teleseismic shear wave splitting measurements above active hot spots.

[53] It is possible that the complex upper mantle structure beneath the caldera scatters energy such that significant *SKS* energy appears on the tangential component without splitting due to anisotropy. Scattering and attenuation are likely to affect the anomalous waveforms recorded within the caldera due to the heterogeneous upper mantle and crust. Scattering could result in nonlinear horizontal particle motions that look like split *S* waves. However, *Alsina and Snieder* [1995] found that scattered energy on the tangential component could not in general be removed by unsplitting the waveforms. In contrast, most (~60%) of the energy on the tangential component in the example for LKWY in Figure 4 is removed by applying the best fit splitting parameters. The overall character of *SKS* waveforms recorded at stations within the caldera is indicative of splitting due to anisotropy rather than scattering.

[54] The large velocity gradients in the upper 200 km beneath Yellowstone (Figure 8) could also affect the apparent splitting measurements there by, for example, severely bending rays out of the plane between source and receiver. We calculated the initial polarization angle of the *SKS* phases after correction for the splitting parameters and found small 5°–10° deviations from the back azimuth direction. The strong velocity gradients beneath the caldera do not appear to have a significant effect on initial polarization estimate.

4.6. Evaluating Models of Plume-Plate Interaction

[55] Shear wave splitting observations have been compared with models of plume-plate interaction at the Hawaiian hot spot [*Walker et al.*, 2001, 2003], the Eifel hot spot [*Walker*, 2004], Iceland [*Bjarnason et al.*, 2002], and the Society hot spot [*Russo and Okal*, 1998]. The basic model that has been used to explain splitting observations at stations within several hundred km of Hawaii and Eifel is based on the expected flow patterns resulting from buoyantly ascending plume material being deflected at the base of a moving plate. A combination of the plate-related shear and radial flow of plume material could produce a parabolic flow pattern and a similar parabolic pattern of splitting fast axes [e.g., *Walker et al.*, 2001]. The parabolic pattern of splitting fast directions in the central Basin and Range (Figure 7) has also been attributed to a possible upwelling there [*Savage and Sheehan*, 2000]. At Iceland, however, the effects of strain related to diverging plates and underlying mantle flow can explain the observed splitting [*Bjarnason et al.*, 2002].

[56] Numerical modeling of the orientation of olivine *a* axes adjacent to plumes indicates the anisotropic fabric might be more complex than the flow lines would indicate [*Rümpker and Silver*, 2000; *Kaminski and Ribe*, 2002]. In particular, the rapid changes in flow directions near the hypothetical plume are not expected to produce a coherent vertical layer of anisotropic material. Because the flow directions are likely to be different at different depths near a plume, observations of near-vertical propagating teleseismic *S* waves at the surface near the plume should have little to no splitting. In addition, *Kaminski and Ribe* [2002] show that for small strains, olivine *a* axes align at approximately 45° to the flow direction and in areas of rapid changes in flow directions, *a* axes align at high angles to the flow directions. While these small-scale changes will not likely be observed in teleseismic *S* waves that average the structure over tens of kilometers, this modeling points to the potential complexity of anisotropy near the model plume.

[57] Farther from the plume where the flow is more uniform, numerical modeling predicts that the *a* axes align with the flow direction; so parabolic asthenosphere flow should be detectable at stations away from the plume [*Kaminski and Ribe*, 2002]. The distance from the plume at which the *a* axes align parallel to flow depends primarily on the velocity of the plate and the amount of plume material ascending and spreading. A low plate velocity combined with a large volume of ascending mantle material would produce a wide parabola.

[58] We modeled parabolic flow in two dimensions as a point source into a uniform stream [*Milne-Thomson*, 1968, p. 211; *Savage and Sheehan*, 2000; *Walker et al.*, 2001]. The uniform streamflow is a proxy for plate motion-induced shear in the asthenosphere, while the point source represents gravitational spreading of buoyant plume material at the base of the plate. The flow direction at the location of each station is computed from interpolation of the flow field.

[59] A model flow field that coincides with the high topography around the ESRP is shown in Figure 9a. This model was designed to correspond with previous models of plume-related flow at Yellowstone by *Sleep* [1990], *Smith and Braile* [1994], and *Lowry et al.* [2000] that use the high topography around the Yellowstone-ESRP system to estimate the extent of plume material. Flow lines are plotted as fine dark lines. The stagnation streamline, representing the separation between plume material and normal mantle [*Sleep*, 1990], is shown with a dark heavy line. The model flow directions at each station are shown as red or green sticks depending on whether the misfit is larger or smaller than 30°. Station average ϕ directions are shown as black sticks. Stations within the caldera, as well as those stations south and east of Yellowstone have the largest errors.

[60] The model with the best fit to the data was found using a grid search over a range of possible combinations of point source location, source strength, and stream velocity (Figure 9b). The best-fit model has a plume in the center of the Yellowstone caldera and a small plume influence on the flow field. The width of the parabola is roughly coincident with the width of the ESRP and much narrower than the topographic high attributed to spreading plume material in earlier studies. Note that the upper mantle low-velocity

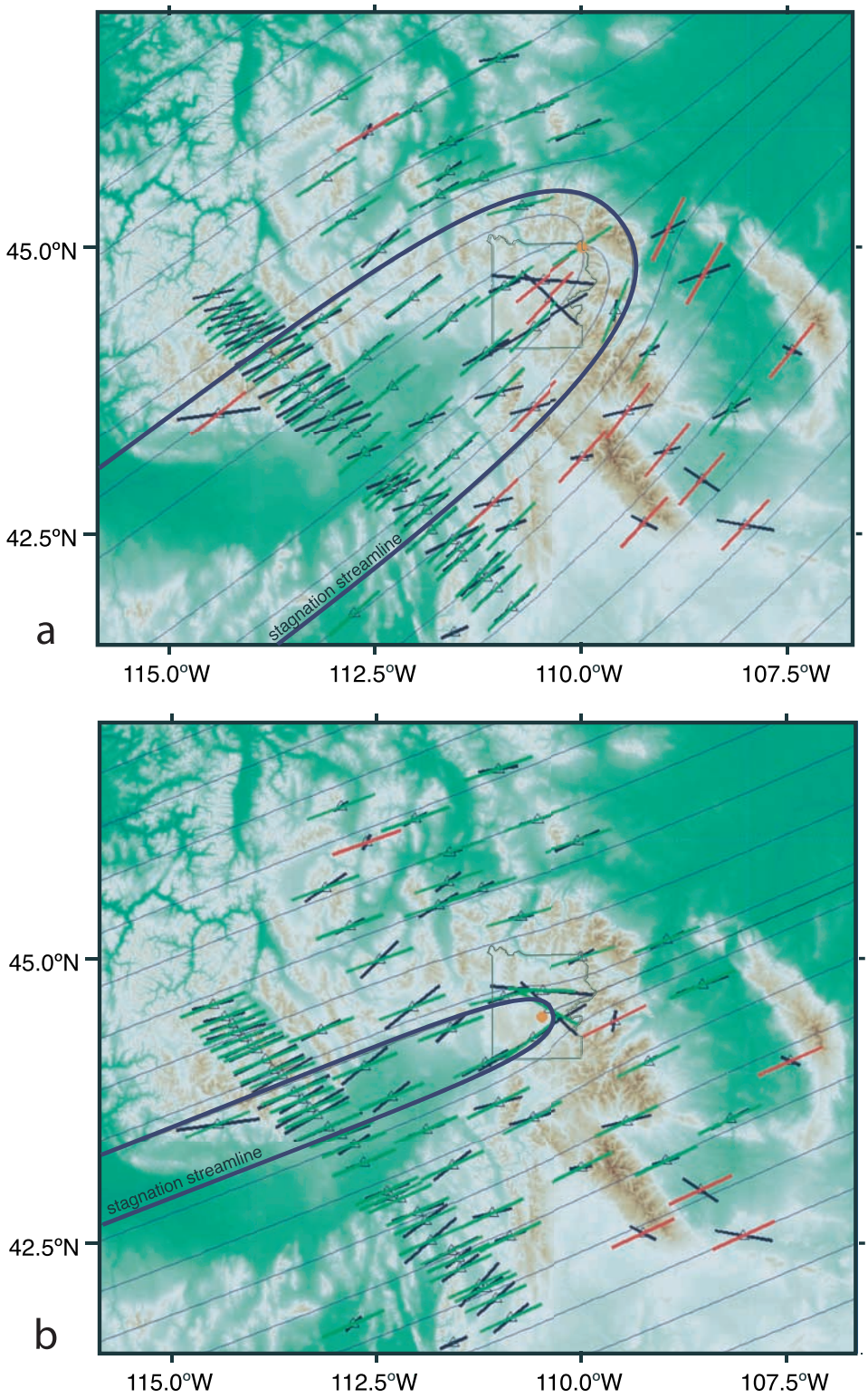

Figure 9. Flow directions at each station are plotted as sticks similar to the sticks used to depict the splitting fast polarization. The sticks are red if they differ from the data by 30° or more. Otherwise, they are green. Station averages are plotted as black sticks. Fine lines depict flow lines, and the dark line represents the stagnation streamline separating plume material from normal mantle. The orange dot shows the location of the plume. The boundary of Yellowstone National Park is shown for reference. (a) A model designed to fit the topography. (b) Best fit model.

anomaly imaged with V_P and V_S tomography is also roughly the width of the ESRP (Figure 8). If this model is correct, the plume material is confined to a downstream area roughly the width of the ESRP. This model is not consistent with the idea that the topographic high around the ESRP is due to buoyant plume material.

4.7. Mantle Flow and Shear Wave Splitting Fast Directions

[61] Most studies of shear wave splitting that explain splitting with simple asthenosphere flow assume that the mantle is stable relative to the moving plate. The direction of maximum strain, olivine *a* axes, and fast anisotropy are presumed to be parallel to the plate motion. If the sub-asthenospheric mantle is convecting, however, the direction of maximum shear, and thus lattice preferred orientation of olivine *a* axes in the asthenosphere might be very different. Recent studies have incorporated mantle velocity into interpretation of splitting fast directions that are different from the absolute plate motion [*Bjarnason et al.*, 2002; *Silver and Holt*, 2002]. The differential motion between the lithosphere, V_L, and mantle at the base of the asthenosphere, V_M produces a LPO fabric by simple shear that has magnitude and direction: $V_L - V_M = V_\phi$.

[62] We compared shear wave splitting ϕ for stations on the ESRP with the direction of absolute plate motion from *Gripp and Gordon* [2002] plus GPS-derived extension on the ESRP [*Puskas et al.*, 2002], and mantle flow models. The ESRP was chosen for this comparison between mantle flow, plate motion and splitting fast axes because the splitting directions on the ESRP are uniform. In addition, the lithosphere beneath the ESRP has likely been reworked by passage over the hot spot and is not expected to have strong fossil anisotropy [*Schutt and Humphreys*, 2001]. Anisotropic fabric in the lithosphere should be relatively simple and reflect recent (<10 Ma) strain.

[63] The ESRP is extending in approximately the direction of plate motion, so we can estimate V_L from the plate motion vector in HS3-NUVEL-1 [*Gripp and Gordon*, 2002] plus the lithosphere deformation vector to get 249° at 2.8 cm/yr. All mantle flow vectors are from modeling by B. Steinberger (personal communication, 2003) [see *Steinberger*, 2000]. In these models, density contrasts in the mantle, which are computed from seismic velocity models, drive mantle flow. In North America, the high-velocity, high-density, sinking Farallon slab, now beneath mid-America, is driving eastward upper mantle flow beneath the western United States [*Bunge and Grand*, 2000]. We compared the plate motion [*Gripp and Gordon*, 2002] with Steinberger's mantle flow fields to predict the asthenosphere LPO.

[64] The mantle velocity predicted by the velocity model of *Grand et al.* [1997] is very small and has little effect on the predicted ϕ. The seismic velocity model of *Su et al.* [1994] predicts ENE mantle velocities on the order of the plate velocity resulting in slightly more easterly oriented V_ϕ. The change in direction is less than 10°, which is within the error on the APM direction. Shear wave fast polarization directions on the ESRP are compatible with differential flow between the North America plate and both of Steinberger's mantle flow models. However, the anisotropy beneath the ESRP can be explained as easily by plate motion over a stationary mantle. We cannot discriminate between Steinberger's mantle models and a stationary upper mantle.

5. Summary

[65] The majority of the shear wave splitting fast axes measured around the Yellowstone hot spot can be interpreted as due to simple shear in the asthenosphere. The nearly uniform direction of splitting fast axes, particularly from stations on and adjacent to the ESRP, is unusual compared to splitting measurements made in the rest of the western United States. The fabric of the asthenosphere and lower lithosphere on the ESRP has likely been reworked by strain and higher temperatures associated with passage over the Yellowstone hot spot. We do not find evidence for radial flow in the asthenosphere found at other hot spots and interpreted to be related to ascending plume material. In particular, the patterns of splitting directions do not match the topographic parabola surrounding Yellowstone and the ESRP. This suggests estimates of a plume buoyancy flux [*Sleep*, 1990; *Lowry et al.*, 2000] at Yellowstone may be too large. If a Yellowstone plume is responsible for the hot spot volcanism, it may be too small, relative to the plate velocity, to be recognized with this technique. Smaller-scale radial flow might be detected in areas adjacent to the Yellowstone caldera if the spatial sampling of shear wave splitting measurements is improved.

[66] Plate motion over a relatively stable mantle is primarily responsible for the anisotropic structure observed. We found that the mantle flow predicted by *Steinberger* [2000] should not significantly affect the direction of fast anisotropy in the asthenosphere. The direction of upper mantle flow beneath Yellowstone is likely nearly parallel to the APM and ϕ directions. Alternatively, the velocity of mantle flow may be much lower than the plate motion velocity so that shear in the asthenosphere is primarily a result of plate motion over a relatively stable mantle.

[67] A striking feature of the splitting data is the rotation of fast axes within the Yellowstone caldera. These ~70° changes in the ϕ orientations are unlikely to reflect asthenosphere fabric because they occur between stations 30 km apart. This is indicative of a shallow source of anisotropy. The large ($\delta t > 2$ s) split times recorded at these stations suggest a high degree of anisotropy. However, splitting measurements at intracaldera stations are relatively sparse, even at the permanent USNSN station LKWY. While we cannot rule out a cause other than anisotropy for the observed tangential *SKS* energy, the data are consistent with anisotropy due to vertical melt lenses in the lithosphere oriented by the strain field.

[68] **Acknowledgments.** We are grateful for the criticism of two anonymous reviewers and Associate Editor David Mainprice. The instruments used in the field program were provided by the PASSCAL facility of IRIS through the PASSCAL Instrument Center. Data collected during this experiment are available through the IRIS Data Management Center. The facilities of the IRIS Consortium are supported by the National Science Foundation under Cooperative Agreement EAR-0004370. Additional data came from the U.S. National Seismograph Network and University of Utah Seismograph Network. Primary financial support for this project came from the National Science Foundation Continental Dynamics Program grants EAR-CD-9725431 and EAR-CD-0314237. G.P.W. was also supported by a University of Utah Graduate Research Fellowship and a U.S. Geological

Survey grant to support the Yellowstone seismic network. Many of the figures were created with GMT [*Wessel and Smith*, 1998].

References

Alsina, D., and R. Snieder (1995), Small-scale sublithospheric continental mantle deformation: Constraints from SKS splitting observations, *Geophys. J. Int.*, *123*, 431–448.

Anders, M. H., and N. H. Sleep (1992), Magmatism and extension: The thermal and mechanical effects of the Yellowstone hotspot, *J. Geophys. Res.*, *97*, 15,379–15,393.

Anders, M. H., J. W. Geissman, L. A. Piety, and J. T. Sullivan (1989), Parabolic distribution of circumeastern Snake River Plain seismicity and latest Quaternary faulting, migratory pattern and association with the Yellowstone hotspot, *J. Geophys. Res.*, *94*, 1589–1621.

Ayele, A., G. Stuart, and J.-M. Kendall (2004), Insights into rifting from shear-wave splitting and receiver functions: An example from Ethiopia, *Geophys. J. Int.*, *157*, 354–362, doi:10.1111/j.1365-246X.2004.02206.x.

Benz, H. M., and R. B. Smith (1984), Simultaneous inversion for lateral velocity variations and hypocenters in the Yellowstone region using earthquake and refraction data, *J. Geophys. Res.*, *89*, 1208–1220.

Bijwaard, H., W. Spakman, and E. R. Engdahl (1998), Closing the gap between regional and global travel time tomography, *J. Geophys. Res.*, *103*, 30,055–30,078.

Bjarnason, I. T., P. G. Silver, G. Rümpker, and S. C. Solomon (2002), Shear wave splitting across the Iceland hot spot: Results from the ICEMELT experiment, *J. Geophys. Res.*, *107*(B12), 2382, doi:10.1029/2001JB000916.

Blackwell, D. D. (1969), Heat-flow determinations in the northwestern United States, *J. Geophys. Res.*, *74*(4), 992–1007.

Bokelmann, G. H., K. T. Walker, and S. L. Klemperer (2003), Shear-wave splitting as a diagnostic tool for resolving plume-related mantle flow around hotspots, *Eos Trans. AGU*, *84*(46), Fall Meet. Suppl., Abstract V21F-01.

Bunge, H.-P., and S. P. Grand (2000), Mesozoic plate-motion history below the northeast Pacific Ocean from seismic images of the subducted Farallon slab, *Nature*, *405*, 337–340.

Christiansen, R. L. (2001), The Quaternary and Pliocene Yellowstone Plateau volcanic field of Wyoming, Idaho, and Montana, *U.S. Geol. Surv. Prof. Pap.*, *729-G*.

Christiansen, R. L., and R. S. Yeats (1992), Post-Laramide geology of the U.S. Cordilleran region, in *The Cordilleran Orogen: Conterminous U.S.*, edited by B. C. Burchfiel, P. W. Lipman, and M. L. Zoback, pp. 261–406, Geol. Soc. of Am., Boulder, Colo.

Christiansen, R. L., G. R. Foulger, and J. R. Evans (2002), Upper-mantle origin of the Yellowstone Hotspot, *Geol. Soc. Am. Bull.*, *114*, 1245–1256.

Craig, H., L. E. Lupton, J. A. Welhan, and R. Poreda (1978), Helium isotope ratios in Yellowstone and Lassen Park volcanic gases, *Geophys. Res. Lett.*, *5*, 897–900.

Crampin, S., and D. C. Booth (1985), Shear-wave polarizations near the North Anatolian Fault, II, Interpretation in terms of crack-induced anisotropy, *Geophys. J. R. Astron. Soc.*, *83*, 75–92.

Crampin, S., and S. Chastin (2003), A review of shear wave splitting in the crack-critical crust, *Geophys. J. Int.*, *155*, 221–240.

Dueker, K. G., and E. D. Humphreys (1990), Upper-mantle velocity structure of the Great Basin, *Geophys. Res. Lett.*, *17*, 1327–1330.

Dueker, K. G., H. Yuan, and B. Zurek (2001), Thick-structured Proterozoic lithosphere of the Rocky Mountain region, *GSA Today*, *11*, 4–9.

Duncan, R. A., and M. A. Richards (1991), Hotspots, mantle plumes, flood basalts, and true polar wander, *Rev. Geophys.*, *29*, 31–50.

Erslev, E. A., and J. F. Sutter (1990), Evidence for Proterozoic mylonitization in the northwestern Wyoming province, *Geol. Soc. Am. Bull.*, *102*, 1681–1694.

Evans, J. R., and H. M. Iyer (1979), Deep structure under Yellowstone and the eastern Snake River plain from teleseismic *P*-wave delays (abstract), *Eos Trans. AGU*, *60*, 942.

Evoy, J. A. (1978), Precision gravity reobservations and simultaneous inversion of gravity and seismic data for subsurface structure of Yellowstone, M.S. thesis, Univ. of Utah, Salt Lake City.

Faul, U. H., D. R. Toomey, and H. S. Waff (1994), Intergranular basaltic melt is distributed in thin, elongated inclusions, *Geophys. Res. Lett.*, *21*, 29–32.

Favela, J., and D. L. Anderson (2000), Extensional tectonics and global volcanism, in *Problems in Geophysics for the New Millennium*, edited by E. Boschi, G. Ekstrom, and A. Morelli, Editrice Compositori, Bologna, Italy.

Fee, D., and K. Dueker (2004), Mantle transition zone topography and structure beneath the Yellowstone hotspot, *Geophys. Res. Lett.*, *31*, L18603, doi:10.1029/2004GL020636.

Fournier, R. O., and A. M. Pitt (1985), The Yellowstone magmatic-hydrothermal system, U.S.A., in *1985 International Symposium on Geothermal Energy: International Volume*, edited by C. Stone, pp. 319–327, Cal Central Press, Sacramento, Calif.

Fox, O. C., A. F. Sheehan, K. G. Dueker, and B. Zurek (2001), Seismic anisotropy across the Cheyenne Belt, southern Wyoming, *Eos Trans. AGU*, *82*(47), Fall Meet. Suppl., Abstract F846.

Gao, S. S., P. M. Davis, H. Liu, P. D. Slack, A. W. Rigor, Y. A. Zorin, V. V. Mordvinova, V. M. Kozhevnikov, and N. A. Logatchev (1997), *SKS* splitting beneath continental rift zones, *J. Geophys. Res.*, *102*, 22,781–22,797.

Goes, S., and S. van der Lee (2002), Thermal structure of the North American uppermost mantle inferred from seismic tomography, *J. Geophys. Res.*, *107*(B3), 2050, doi:10.1029/2000JB000049.

Grand, S. P., R. D. Van der Hilst, and S. Widiyantoro (1997), Global seismic tomography: A snapshot of convection in the Earth, *GSA Today*, *7*, 1–7.

Gripp, A. E., and R. G. Gordon (2002), Young tracks of hotspots and current plate velocities, *Geophys. J. Int.*, *150*, 321–361.

Hammond, W. C., and E. D. Humphreys (2000), Upper mantle seismic wave velocity: Effects of realistic partial melt geometries, *J. Geophys. Res.*, *105*, 10,975–10,986.

Hartog, R., and S. Y. Schwartz (2001), Depth-dependent mantle anisotropy below the San Andreas fault system; apparent splitting parameters and waveforms, *J. Geophys. Res.*, *106*, 4155–4167.

Holtzman, B. K., D. L. Kohlstedt, M. E. Zimmerman, F. Heidelbach, T. Hiraga, and J. Hustoft (2003), Melt segregation and strain partitioning: Implications for seismic anisotropy and mantle flow, *Science*, *301*, 1227–1230.

Humphreys, E. D., and K. G. Dueker (1994a), Physical state of the western U.S. upper mantle, *J. Geophys. Res.*, *99*, 9635–9650.

Humphreys, E. D., and K. G. Dueker (1994b), Western U.S. upper mantle structure, *J. Geophys. Res.*, *99*, 9615–9634.

Humphreys, E. D., K. G. Dueker, D. L. Schutt, and R. B. Smith (2000), Beneath Yellowstone; evaluating plume and nonplume models using teleseismic images of the upper mantle, *GSA Today*, *10*, 1–7.

Husen, S., R. B. Smith, and G. P. Waite (2004), Evidence for gas and magmatic sources beneath the Yellowstone Volcanic Field from seismic tomographic imaging, *J. Volcanol. Geotherm. Res.*, *131*, 397–410, doi:10.1016/S0377-0273(03)00416-5.

Iyer, H. M., J. R. Evans, G. Zandt, R. M. Stewart, J. M. Coakley, and J. N. Roloff (1981), A deep low-velocity body under the Yellowstone caldera, Wyoming: Delineation using teleseismic P-wave residuals and tectonic interpretation, *Geol. Soc. Am. Bull.*, *92*, 792–798, 1471–1646.

Jordan, M., R. B. Smith, and G. P. Waite (2004), Tomographic images of the Yellowstone hotspot structure, *Eos Trans. AGU*, *85*(47), Fall Meet. Suppl., Abstract V51B-0556.

Jung, H., and S. Karato (2001), Water-induced fabric transitions in olivine, *Science*, *293*, 1460–1463.

Kaminski, É., and N. M. Ribe (2002), Timescales for the evolution of seismic anisotropy in mantle flow, *Geochem. Geophys. Geosyst.*, *3*(8), 1051, doi:10.1029/2001GC000222.

Karlstrom, K., et al. (2002), Structure and evolution of the lithosphere beneath the Rocky Mountains: Initial results from the CD-ROM experiment, *GSA Today*, *12*, 4–10.

Kendall, J.-M. (1994), Teleseismic arrivals at a mid-ocean ridge; effects of mantle melt and anisotropy, *Geophys. Res. Lett.*, *21*, 301–304.

Kendall, J.-M., G. W. Stuart, C. J. Ebinger, I. D. Bastow, and D. Keir (2005), Magma-assisted rifting in Ethiopia, *Nature*, *433*, 146–148, doi:10.1038/nature03161.

Lehman, J. A., R. B. Smith, M. M. Schilly, and L. W. Braile (1982), Upper crustal structure of the Yellowstone caldera from delay time analyses and gravity correlations, *J. Geophys. Res.*, *87*, 2713–2730.

Levin, V., W. Menke, and J. Park (1999), Shear wave splitting in the Appalachians and the Urals: A case for multilayered anisotropy, *J. Geophys. Res.*, *104*, 17,975–17,993.

Lowry, A. R., N. L. Ribe, and R. B. Smith (2000), Dynamic elevation of the Cordillera, western United States, *J. Geophys. Res.*, *105*, 23,371–23,390.

Menke, W. (1989), *Geophysical Data Analysis: Discrete Inverse Theory*, Elsevier, New York.

Miller, D. S., and R. B. Smith (1999), *P* and *S* velocity structure of the Yellowstone volcanic field from local earthquake and controlled-source tomography, *J. Geophys. Res.*, *104*, 15,105–15,121.

Milne-Thomson, L. M. (1968), *Theoretical Hydrodynamics*, 5th ed., 743 pp., Macmillan, New York.

Montelli, R., G. Nolet, F. A. Dahlen, G. Masters, E. R. Engdahl, and S.-H. Hung (2004), Finite-frequency tomography reveals a variety of plumes in the mantle, *Science*, *303*, 338–343, doi:10.1126/science.1092485.

Morgan, W. J. (1971), Plate motions and deep mantle convection, *Nature*, *230*, 42–43.

Pelton, J. R., and R. B. Smith (1982), Contemporary vertical surface displacements in Yellowstone National Park, *J. Geophys. Res.*, *87*, 2745–2761.

Perkins, M. E., and B. P. Nash (2002), Explosive silicic volcanism of the Yellowstone hotspot: The ashfall tuff record, *Geol. Soc. Am. Bull.*, *114*, 367–381.

Pierce, K. L., and L. A. Morgan (1992), The track of the Yellowstone hot spot; volcanism, faulting, and uplift, in *Regional Geology of Eastern Idaho and Western Wyoming*, edited by P. K. Link, M. A. Kuntz, and L. B. Platt, *Mem. Geol. Soc. Am.*, *179*, 1–53.

Polet, J., and H. Kanamori (2002), Anisotropy beneath California; shear wave splitting measurements using a dense broadband array, *Geophys. J. Int.*, *149*(2), 313–317.

Puskas, C. M., R. B. Smith, and C. M. Meertens (2002), GPS-derived models of intraplate deformation of the Yellowstone hotspot, *Eos Trans. AGU*, *83*(47), Fall Meet. Suppl., Abstract F1037.

Rümpker, G., and T. Ryberg (2000), New "Fresnel-zone" estimates for shear-wave splitting observations from finite-difference modeling, *Geophys. Res. Lett.*, *27*, 2005–2008.

Rümpker, G., and P. G. Silver (2000), Calculating splitting parameters for plume-type anisotropic structures of the upper mantle, *Geophys. J. Int.*, *143*, 507–520.

Russo, R. M., and E. A. Okal (1998), Shear wave splitting and upper mantle deformation in French Polynesia: Evidence for small-scale heterogeneity related to the Society hotspot, *J. Geophys. Res.*, *103*, 15,089–15,107.

Sandvol, E., and T. Hearn (1994), Bootstrapping shear-wave splitting errors, *Bull. Seismol. Soc. Am.*, *84*, 1971–1977.

Savage, M. K., and A. F. Sheehan (2000), Seismic anisotropy and mantle flow from the Great Basin to the Great Plains, western United States, *J. Geophys. Res.*, *105*, 13,715–13,734.

Schutt, D. L., and E. D. Humphreys (2001), Evidence for a deep asthenosphere beneath North America from western United States *SKS* splits, *Geology*, *29*, 291–294.

Schutt, D. L., and E. D. Humphreys (2004), *P* and *S* wave velocity and V_P/V_S in the wake of the Yellowstone hot spot, *J. Geophys. Res.*, *109*, B01305, doi:10.1029/2003JB002442.

Schutt, D. L., E. D. Humphreys, and K. G. Dueker (1998), Anisotropy of the Yellowstone Hot Spot wake, eastern Snake River Plain, Idaho, *Pure Appl. Geophys.*, *151*, 443–462.

Silver, P. G. (1996), Seismic anisotropy beneath the continents: Probing the depths of geology, *Annu. Rev. Earth Planet. Sci.*, *24*, 385–432.

Silver, P. G., and W. W. Chan (1991), Shear wave splitting and subcontinental mantle deformation, *J. Geophys. Res.*, *96*, 16,429–16,454.

Silver, P. G., and W. E. Holt (2002), The mantle flow field beneath western North America, *Science*, *295*, 1054–1057.

Silver, P. G., and M. K. Savage (1994), The interpretation of shear-wave splitting parameters in the presence of two anisotropic layers, *Geophys. J. Int.*, *119*, 949–963.

Sleep, N. H. (1990), Hotspots and mantle plumes: Some phenomenology, *J. Geophys. Res.*, *95*, 6715–6736.

Smith, D. A., and D. G. Milbert (1999), The GEOID96 high-resolution geoid height model for the United States, *J. Geod.*, *73*, 219–236.

Smith, P. G., and G. Ekström (1999), A global study of *Pn* anisotropy beneath continents, *J. Geophys. Res.*, *104*, 963–980.

Smith, R. B., and L. W. Braile (1994), The Yellowstone hotspot, *J. Volcanol. Geotherm. Res.*, *61*, 121–187.

Smith, R. B., and M. L. Sbar (1974), Contemporary tectonics and seismicity of the western United States with emphasis on the Intermountain Seismic Belt, *Geol. Soc. Am. Bull.*, *85*, 1205–1218.

Steinberger, B. (2000), Plumes in a convecting mantle: Models and observations for individual hotspots, *J. Geophys. Res.*, *105*, 11,127–11,152.

Su, W.-J., R. L. Woodward, and A. M. Dziewonski (1994), Degree 12 model of shear velocity heterogeneity in the mantle, *J. Geophys. Res.*, *99*, 6945–6980.

Waite, G. P., and R. B. Smith (2004), Seismotectonics and stress field of the Yellowstone volcanic plateau from earthquake first motions and other indicators, *J. Geophys. Res.*, *109*, B02301, doi:10.1029/2003JB002675.

Waite, G. P., R. B. Smith, C. M. Puskas, D. L. Schutt, and R. M. Allen (2003), Kinematics of the Yellowstone Hotspot derived from seismic anisotropy, tomography, and GPS, *Geophys. Res. Abstr.*, *5*, Abstract EAE03-A-00670.

Waite, G. P., R. B. Smith, C. M. Puskas, and D. L. Schutt (2004), Interpreting crust and mantle stress and strain indicators at Yellowstone, *Eos Trans. AGU*, *85*(47), Fall Meet. Suppl., Abstract T33E-07.

Walker, K. T. (2004), Exploring Problems in tectonics and geodynamics with seismology, Ph.D. thesis, Stanford Univ., Palo Alto, Calif.

Walker, K. T., G. H. R. Bokelmann, and S. L. Klemperer (2001), Shear-wave splitting to test mantle deformation models around Hawaii, *Geophys. Res. Lett.*, *28*, 4319–4322.

Walker, K. T., G. H. R. Bokelmann, and S. L. Klemperer (2003), Reply to comment by L.P. Vinnik et al. on "Shear-wave splitting to test mantle deformation models around Hawaii", *Geophys. Res. Lett.*, *30*(13), 1676, doi:10.1029/2002GL016712.

Wessel, P., and W. H. F. Smith (1998), New, improved version of the Generic Mapping Tools released, *Eos Trans. AGU*, *79*, 579.

Wicks, C. W., W. R. Thatcher, and D. Dzurisin (1998), Migration of fluids beneath Yellowstone caldera inferred from satellite radar interferometry, *Science*, *282*, 458–462.

D. L. Schutt, Department of Geology and Geophysics, University of Wyoming, 1000 University Ave., Laramie, WY 82071, USA.

R. B. Smith, Department of Geology and Geophysics, University of Utah, 135 S. 1460 E., Salt Lake City, UT 84112, USA.

G. P. Waite, U.S. Geological Survey, 345 Middlefield Road, MS 910, Menlo Park, CA 94025, USA. (gwaite@usgs.gov)